Modeling low saline carbonated water flooding including surface complexes

Alvarez, A. C.; Bruining, J.; Marchesin, D.

DOI
10.1007/s10596-024-10274-1

Publication date
2024

Document Version
Final published version

Published in
Computational Geosciences

Citation (APA)
Alvarez, A. C., Bruining, J., & Marchesin, D. (2024). Modeling low saline carbonated water flooding including surface complexes. *Computational Geosciences*, *28*(3), 373-393. https://doi.org/10.1007/s10596-024-10274-1

Computational Geosciences
https://doi.org/10.1007/s10596-024-10274-1

ORIGINAL PAPER

Modeling low saline carbonated water flooding including surface complexes

A.C. Alvarez[1] · J. Bruining[2] · D. Marchesin[3]

Received: 9 May 2023 / Accepted: 13 January 2024

Abstract
Carbonated water flooding (CWI) increases oil production due to favorable dissolution effects and viscosity reduction. Accurate modeling of CWI performance requires a simulator with the ability to capture the true physics of such process. In this study, compositional modeling coupled with surface complexation modeling (SCM) are done, allowing a unified study of the influence in oil recovery of reduction of salt concentration in water. The compositional model consists of the conservation equations of total carbon, hydrogen, oxygen, chloride and decane. The coefficients of such equations are obtained from the equilibrium partition of chemical species that are soluble both in oleic and the aqueous phases. SCM is done by using the PHREEQC program, which determines concentration of the master species. Estimation of the wettability as a function of the Total Bound Product (TBP) that takes into account the concentration of the complexes in the aqueous, oleic phases and in the rock walls is performed. We solve analytically and numerically these equations in 1−D in order to elucidate the effects of the injection of low salinity carbonated water into a reservoir containing oil equilibrated with high salinity carbonated water.

Keywords Surface complexation modeling · Wettability · Carbonate water flooding · Conservation laws

1 Introduction

Carbonated Water Injection (CWI) is an oil recovery technique that increases the oil production due to favorable dissolution effects causing viscosity reduction [9, 19]. When this method is combined with low salinity brine injection, the brine behaves like a natural solvent that enhances oil recovery [17, 54]. In this way CWI takes advantage of brine flooding to improve oil recovery from 5 to 20% of the oil initially in place (OIIP) [27, 40, 63]. This happens because geochemical reactions between the injected carbonated brine and rock can alter the petrophysical properties of the reservoir.

While there are several studies showing the relevance of CWI coreflood for enhanced oil recovery, understanding such process is still a challenge. Among such processes are the effects of wettability, the flow of mineral salts in water and flow of CO_2 in the aqueous and oleic phases. In this paper, we use multiphase compositional modeling to quantify the oil and water saturations as well as the CO_2 transfer between the aqueous and oleic phases. As novelty we take into account the formation of surface complexes, which participate in the mechanism of wettability modification due to charge transfer [7, 35]. With this new effect we can quantify the intrinsic nonlinear relation leading to optimal recovery conditions. We also evaluate the modifications of pH, of the velocity of the saline front and of the magnitude of the saturation shock. These changes are the main factors for the increase in oil productivity.

Modeling enhanced oil recovery (EOR) by conventional fractional−flow theory [16, 45] has had numerous extensions to take into account different mechanisms that contribute to injectivity. Some model extensions have included CO_2 [18,

A.C. Alvarez, J. Bruining and D. Marchesin contributed equally to this work.

✉ A.C. Alvarez
amaury@ic.ufrj.br

J. Bruining
J.Bruining@tudelft.nl

D. Marchesin
marchesi@impa.br

[1] Instituto de Computação, Universidade Federal do Rio de Janeiro, Avenida Athos da Silveira Ramos, 274, Rio de Janeiro 21941-590, Rio de Janeiro, Brasil

[2] Lab. Fluid Dynamics, IMPA, Estrada Dona Castorina, 110, Rio de Janeiro 22460-320, Rio de Janeiro, Brasil

[3] Civil Engineering and Geosciences, TU Delft, Stevinweg 1, Delft 2628 CE, Delft, The Netherlands

Published online: 01 February 2024

59, 66] and molecular diffusion [30]. Thus compositional modeling has been developed to include master chemical species in the aqueous and oleic phases [26, 64]. More recently some authors have included in the model the transport of ions [1, 6, 61]. Some authors emphasize that surface complex formation is a mechanism responsible for increased oil recovery [3]. It has often been stated that the injection of water with low salinity and CO_2 produces chemical reactions that change wettability of rock walls favorable to enhanced oil recovery [36].

Some research underlines that wettability alteration changes the oil recovery when carbonated water at low salinity is injected, see, e.g., [69, 70]. Understanding this recovery method is one of the purposes of this work, for conditions typical of the Brazilian pre-salt basin.

In [33] it is highlighted that the formation of surface complexes contributes to changes in wettability. This happens because charges on the calcite and oleic surfaces have opposite signs, which contributes to squeezing out the water film; this effect forms an oil-wet surface [31]. This effect can be explained in terms of changes in pH values and of larger shock amplitudes in the saturation profile. Understanding this phenomenon is an expected result of this work.

To incorporate this process, we use multiphase compositional modeling with master species. We consider the concentrations of ions generated by all equilibrium reactions present in the carbonated brine and CO_2 in the aqueous and oleic phases. To do so, we use a one dimensional incompressible flow model that describes two-phase flow with geochemical modeling ([26]). These processes are studied by means of a system of balance laws for the transported quantities. Using this model we study the flow of oil, water and dissolved carbon dioxide in a sandstone rock.

The geochemical data are obtained by utilizing the modeling capabilities of the program PHREEQC (acronym of pH-REdox-Equilibrium C-program). This is a computer program written in C++ designed to perform a wide variety of aqueous geochemical calculations (see details about its implementation in [7, 8, 57, 58]). Furthermore, we use the program for calculation of the surface complexation in calcite rock [65]. The program determines the concentration of ions and molecules dissolved in water inclusive carbon dioxide (CO_2), which is the only compound that exists in both phases. By assuming chemical equilibrium, we define the behavior of all dissolved compounds by means of four transport equations of master species, which are chloride, oil, twice oxygen minus hydrogen and inorganic carbon.

We also consider the ions (H^+, OH^-, CO_3^{2-}, HCO_3^-, Cl^-), water (H_2O) and the sorbed species oil_{s,NH^+}, $oil_{w,COOH}$, $Cal_{s,OH}$, Cal_{w,CO_3H}, $oil_{s,N}$, oil_{w,COO^-}, $oil_{w,COOCa^+}$, Cal_{s,OH_2^+}, Cal_{s,CO_3^-}, Cal_{w,CO_3^-}, Cal_{w,CO_3Ca^+} [12]. The species with complexes lead to what we call the surface complexes−chloride ionic carbon dioxide−oil−water SC-CLICDOW model. This model summarizes the most relevant concepts described in [14, 15, 32, 41, 42]. To illustrate these effects we inject water with the same pH but with lower salinity than the initial salinity in the core.

In this study, we use SCM through the geochemistry PHREEQC program. This solver is utilized to calculate the concentration of the complexes and to predict the wettability alteration of minerals through the Total Bound Product (TBP). Details of the procedure employed here can found in [51]. SCM is a chemical equilibrium technique used to model the interactions of water, oil, brine and rock [23, 23, 49]. Such a method has been used in several studies for characterizing the surface adsorption phenomenon [50, 60] and determining the wettability of minerals at reservoir conditions [11, 28, 51].

In these works the model is based on adsorption of aqueous solute into surface functional groups characterized by a set of chemical reactions. Moreover, some experiments indicate that since carbonates are salt-type minerals, their surface reactivity is different from sandstone and clays. Another conclusion is that dissolution and precipitation interfere on ion adsorption dynamics at functional sites. The main effects that influence the oil-brine-rock interaction are the brine chemistry and the oil composition, i.e., acid and base number [20].

Several works describe how to quantity the relationship between salt concentration and water flooding process, e.g., [2, 35, 56]. In this paper we use a similar idea, which is proposed by [35] utilizing the relative permeability functions based on Corey's correlation.

Based on Gibbs rule and assuming that the sodium and chloride concentrations are approximately equal, we consider four balance laws, i.e., total carbon, hydrogen−oxygen, chloride and decane. Each one consists of three terms, i.e., accumulation, convection and the combination of molecular and capillary diffusion. In this way, we obtain analytically the Riemann solution, which consists basically in applying the method of characteristics (MOC) through the wave curve method. In this work we use this method to seek analytical solutions of the SC−CLICDOW model similar to the model treated in [1, 16, 18, 21, 37, 45, 59, 66]. The Riemann solution consists of a concatenation of spreading and shock waves, implementing certain admissibility conditions ([29, 44, 46, 47, 55]).

A Riemann solver for the proposed geochemical model is developed to quantify the geochemical processes of water injection with CO_2 and low salinity in a carbonated reservoir. We also take into account the surface complexes formation as a mechanism to change wettability.

A Riemann solver is developed to automate the construction of solution paths. To do so, we take into account the bifurcation structures, which are not part of the classical fractional flow method used by [59]. We also provide comparisons with numerical solutions obtained by means

of a commercial program (COMSOL). This procedure is extremely useful because it allows to include in a unified manner the geochemistry, the equilibrium reactions and the charge balances. Also, the method serves to study different situations and to include more chemical species in the system. Using the extended Gibbs rule (see Eq. (1)), we reduce the mathematical complexity associated with considering the large number of physical constraints and parameters that are included in the geochemistry program PHREEQC.

We use a similar methodology as developed in [1, 6] where the extended Gibbs phase rule was used to focus on the principal chemical species and to incorporate the geochemistry of the oil recovery. This circumvents simultaneous solution of the transport equations, of the equilibrium relations and of the effect of low salt concentrations.

The aims on this paper are (1) to quantify how the presence of surface complexes affects wettability (2) to understand how changes in the salt concentration affects relative permeability and as a consequence of the injectivity (3) to analyze the wave structure of the solutions (e.g., the occurrence of a pH wave embedded in a constant pH flood), front salt formation and a jump in water saturation. The Riemann solution confirms that pH variations occur with various numerical schemes, inclusive discontinuous Galerkin, which is expected when surface complexes are formed.

The additional advantage of the Riemann solution is that it can be used to perform a bifurcation analysis, and to make an inventory of the possible qualitatively different solutions. The bifurcations occur at coincidence and inflection loci. Clearly, bifurcations are essential to build the analytical solution, as well as to determine the location where qualitative changes of the behavior of the solution are expected. This determination is a useful tool for mathematical modeling in oil recovery.

By means of numerical and analytical methods we aim in this paper at quantifying the recovery improvement when carbonated water at low salinity is injected in a reservoir that contains carbonated brine in equilibrium with an oleic phase and carbon dioxide.

For the fulfillment of the objectives our paper is organized as follows. Section 2 gives the physical model and the equilibrium equations considered in this study. In Section 3 the derivation of the mass balance equations for master species are presented. Moreover, Corey parameters of the flow functions depending on salt concentration is presented. In Section 4 a summary of the surface complexation model is presented together with values of the parameters considered in this study. Besides, regression formulas for parameters of the system of conservation laws depending on pH and chloride concentration are presented. Furthermore, a procedure for the calculation of wettability depending on TBP is described. Section 5 outlines the coupled modeling approach integrating carbonated water injection (CWI) with CO2, low salinity injection, and Surface Complexation Modeling (SCM). Section 6 describes the Riemann solver and the strategy to obtain the Riemann solution. Section 7 gives the results in terms of the pH, the chloride concentration, the water saturation and the total velocity. The calculation suggests that a low salinity carbonated water flood improves the recovery because it admits a high dissolved concentration of carbon dioxide.

2 Physical model

We consider the injection of low salinity brine ($0.5\,mol/liter$ NaCl, saturated with CO_2 at a $pH = 4.0$) into an inert rock filled with an oleic phase. Injection and initial fluids contain carbon dioxide and other unrelated ions such as sodium chloride. We assume chemical equilibrium in both the aqueous phase and the oleic phase [1]. The ions and water are only present in the aqueous phase, decane is only present in the oleic phase. Indeed, dissolution of oil in the aqueous phase is disregarded. The solubility of carbon dioxide decreases dramatically at high salt concentration. We assume that the flow is governed by Darcy's law. The temperature is chosen to be 39^oC because literature data is available and the pressure is chosen to be well above the pressure at which a gaseous phase can exist.

We apply the extended Gibbs phase rule to determine the number of degrees of freedom n_f. This rule states (see, e.g., [34, 53]) that this number is given by

$$n_f = N_s + n_s - N_r - n_c + 2 - p, \tag{1}$$

where N_s is the number of dissolved chemical species, n_s is the number of surface species, N_r is the number of chemical reactions and n_c is the number of constraints, e.g., the charge balance. The number 2 represents the temperature and pressure and p the number of phases.

We follow Appelo and Parkhurst [7, 58] and obtain with the geochemistry program PHREEQC, when we add water, $CaCO_3\,(solid)$ and $NaCl$, that there are fifteen different chemical species ($N_s = 15$) with molar concentrations in the aqueous phase: c_{a,CO_2}, $c_{a,CO_3^{2-}}$, c_{a,HCO_3^-}, $c_{a,CaHCO_3^+}$, $c_{a,CaCO_3}$, $c_{a,NaCO_3^-}$, $c_{a,NaHCO_3}$, c_{a,H_2O}, c_{a,H^+}, c_{a,OH^-}, $c_{a,CaOH^+}$, $c_{a,Ca^{2+}}$, c_{a,Cl^-}, c_{a,Na^+} and the alkane (A) concentration in the oleic phase $c_{o,A}$. The alkane only occurs in the oleic phase, whereas all the other components occur only in the aqueous phase. $CaCO_3$ occurs both in the solid phase with concentration $c_{r,CaCO_3}$ and in the aqueous phase with concentration $c_{a,CaCO_3}$. In addition we have $n_s = 11$ sorbed species oil_{s,NH^+}, $oil_{w,COOH}$, $Cal_{s,OH}$, Cal_{w,CO_3H}, $oil_{s,N}$, oil_{w,COO^-}, $oil_{w,COOCa^+}$, Cal_{s,OH_2^+}, Cal_{s,CO_3^-}, Cal_{w,CO_3^-}, Cal_{w,CO_3Ca^+}. There are seven surface reactions

taking into account complexes. These surface reactions are [12]

$$\begin{aligned}
oil_{s,NH^+} &\rightleftharpoons oil_{s,N} + H^+ && \log K_{-11} = -6.0\\
oil_{w,COOH} &\rightleftharpoons oil_{w,COO^-} + H^+ && \log K_{-21} = -5.0\\
oil_{w,COOH} + Ca^{2+} &\rightleftharpoons oil_{w,COOCa^+} + H^+ && \log K_{22} = -3.8\\
Cal_{s,OH} + H^+ &\rightleftharpoons Cal_{s,OH_2^+} && \log K_{13} = 11.8\\
Cal_{s,OH} + HCO_3^- &\rightleftharpoons Cal_{s,CO_3^-} + H_2O && \log K_{33} = 5.8\\
Cal_{w,CO_3H} &\rightleftharpoons Cal_{w,CO_3^-} + H^+ && \log K_{-14} = -5.1\\
Cal_{w,CO_3H} + Ca^{2+} &\rightleftharpoons Cal_{w,CO_3Ca^+} + H^+ && \log K_{24} = -2.6 \quad (2)
\end{aligned}$$

We use four different sorption sites. Each of the sorption sites can receive sorption molecules of two types, called *weak* and *strong*. For instance the strong adsorption sites in oil can receive both oil_{s,NH^+} and $oil_{s,N}$, so that the sum of the sorbed concentration at each sorption site is a given constant. A similar situation occurs for the weak adsorption sites on oil (oil_s), but now with three surface species. The concentration of $CaCO_3$ in the solid phase is known and constant. Thus taking into account the charge balance equation we have $n_c = 5$ constraints.

We notice that the species can be derived from seven master species, i.e., $C\ (4)$, $H\ (1)$, $O\ (-2)$, $Ca(2)$, $Na(1)$, $Cl\ (-1)$, $C\ (-4)$, where the value in parentheses denotes the constant valence of the species. We note that $C\ (-4)$ is used to denote organic carbon as opposed to $C\ (4)$, which denotes inorganic carbon.

We consider the following eight equilibrium reactions in the aqueous phase (thus we have $N_r = 15$)

$$(CO_2)_{aq} + H_2O \rightleftharpoons HCO_3^- + H^+$$

$$HCO_3^- \rightleftharpoons CO_3^{2-} + H^+$$

$$H_2O \rightleftharpoons OH^- + H^+$$

$$(CaCO_3)_{aq} \rightleftharpoons Ca^{2+} + CO_3^{2-}$$

$$Ca^{2+} + H_2O \rightleftharpoons CaOH^+ + H^+$$

$$CO_3^{2-} + Ca^{2+} + H^+ \rightleftharpoons CaHCO_3^+$$

$$Na^+ + CO_3^{2-} \rightleftharpoons NaCO_3^-$$

$$Na^+ + HCO_3^- = NaHCO_3$$

We dropped the subscript (aq) on all compounds except $CaCO_3$ and CO_2 as we assume that they only occur in the aqueous phase. All possible equilibrium equations can be derived from these eight equilibrium reactions.

Thermodynamic equilibrium requires that the chemical potential of $(CaCO_3)_r$ in the solid phase is equal to the chemical potential of $(CaCO_3)_{aq}$ in the aqueous phase. This can be represented by

$$(CaCO_3)_r \rightleftharpoons (CaCO_3)_{aq}\,. \tag{3}$$

In the same way the chemical potential of carbon dioxide in the aqueous phase is equal to the chemical potential in the oleic phase. This can be represented as

$$(CO_2)_o \rightleftharpoons (CO_2)_{aq}\,. \tag{4}$$

As we consider solid, aqueous and oleic phases, the number of phases p is 3. We have the charge balance equation given by

$$\begin{pmatrix} 2c_{a,CO_3} + oil_{w,COO^-} + c_{a,HCO_3} + c_{a,OH} + c_{a,NaCO3} + c_{a,Cl} \\ +Cal_{s,CO_3^-} + Cal_{w,CO_3^-} = 2c_{a,Ca} + oil_{s,NH^+} \\ +c_{a,H} + c_{a,Ca(HCO_3)} + c_{a,Na} + c_{a,CaOH} + oil_{w,COOCa^+} \\ +Cal_{s,OH_2^+} + Cal_{w,CO_3Ca^+} \end{pmatrix}.$$

This charge balance equation can also be derived from the mass balance equations. Thus, we adopt the charge balance equation allowing one mass balance equation to be removed.

Following Gibbs rule described in (1) the number n_f of degrees of freedom is

$$n_f = N_s + n_s - N_r - n_c - p + 2 = 15 + 11 - 15 - 5 - 3 + 2 = 5. \tag{5}$$

In Eq. 5 we use that $N_s + n_s - N_r - n_c = 6$. Given the temperature and pressure, we only need three concentrations to specify the composition of the three phase system.

For the independent concentrations we choose the hydrogen ion c_{a,H^+}, concentration the chloride ion c_{a,Cl^-} concentration and the sodium ion concentration c_{a,Na^+}. Another assumption consists in taking the chloride and sodium ion concentration as equal. This assumption is to simplify our model.

3 Mass balance equations for porous medium flow with surface species

All compounds that are used in the model are built with the atoms $C\ (4)$, $H\ (1)$, $O\ (-2)$, $Ca\ (2)$, $Na\ (1)$, $Cl\ (-1)$ and $C\ (-4)$. For instance carbon dioxide consists of one atom of carbon with valence four and two oxygen atoms with valence minus two. The uncompensated valences result in the charge of the ion, e.g., CO_3^{-2} consists of one atom $C\ (4)$ and three oxygen atoms $O\ (-2)$. Hence CO_3^{2-} has a charge of minus 2. Organic carbon is denoted by $C\ (-4)$, leading to for instance CH_4, where the four valent carbon is compensated by four monovalent hydrogens. Two carbons may

combine to C_2 (-6), and n carbons to C_n $(-2n-2)$, but we denote all organic carbon by C (-4).

The concentrations of all species are expressed in term of activities and activity coefficients, where the activity coefficients γ depend only on the ionic strength μ.

3.1 Master species in terms of activities in the aqueous phase

For the derivation of the mass balance equation we first derive the equations for the dissolved master species, i.e., C (4), H (1), O (-2), Ca (2), Cl (-1), Na (1) concentrations in the aqueous solution, which do not include the surface master species.

For convenience we first define the total aqueous inorganic carbon (i.e., without hydrocarbon) concentration $C_{a,C(4)}$ by

$$C_{a,C(4)} := \frac{a_{a,CO_2}}{\gamma_{a,CO_2}(\mu)} + \frac{a_{a,CO_3^{2-}}}{\gamma_{a,CO_3^{2-}}(\mu)} + \frac{a_{a,HCO_3^-}}{\gamma_{a,HCO_3^-}(\mu)} + \frac{a_{a,CaHCO_3^+}}{\gamma_{a,CaHCO_3^+}(\mu)} + \frac{a_{a,CaCO_3}}{\gamma_{a,CaCO_3}(\mu)} + \frac{a_{a,NaCO_3^-}}{\gamma_{a,NaCO_3^-}(\mu)} + \frac{a_{a,NaHCO_3}}{\gamma_{a,NaHCO_3}(\mu)}. \quad (6)$$

In the same way we define the total aqueous hydrogen concentration by

$$C_{a,H(1)} := \left(\begin{array}{c} 2\frac{a_{a,H_2O}}{\gamma_{a,H_2O}} + \frac{a_{a,H^+}}{\gamma_{a,H^+}(\mu)} + \frac{a_{a,OH^-}}{\gamma_{a,OH^-}(\mu)} \\ + \frac{a_{a,HCO3^-}}{\gamma_{a,OH^-}(\mu)} + \frac{a_{a,CaHCO_3^+}}{\gamma_{a,CaHCO_3^+}(\mu)} + \frac{a_{a,CaOH+}}{\gamma_{a,CaHCO_3^+}(\mu)} + \\ \frac{a_{a,NaHCO_3}}{\gamma_{a,CaHCO_3^+}(\mu)} \end{array} \right) := 2\frac{a_{a,H_2O}}{\gamma_{a,H_2O}} + \delta C_{a,H(1)}. \quad (7)$$

where the concentration of water $c_{a,H_2O} = a_{a,H_2O}/\gamma_{a,H_2O}$ is much larger than the other concentrations.

The total aqueous oxygen concentration can be written as

$$C_{a,O(-2)} := \left(\begin{array}{c} \frac{a_{a,H_2O}}{\gamma_{a,H_2O}} + \frac{3a_{a,CO_3^{2-}}}{\gamma_{a,CO_3^{2-}}(\mu)} + \frac{a_{a,OH^-}}{\gamma_{a,OH^-}(\mu)} + \frac{2a_{a,CO2}}{\gamma_{a,CO2}(\mu)} \\ + \frac{3a_{a,HCO3^-}}{\gamma_{a,HCO3^-}(\mu)} + \frac{3a_{a,CaHCO_3^+}}{\gamma_{a,CaHCO_3^+}(\mu)} + \frac{a_{a,CaOH^+}}{\gamma_{a,CaOH^+}(\mu)} + \\ + \frac{3a_{a,CaCO_3}}{\gamma_{a,CaCO_3}(\mu)} + \frac{3a_{a,NaCO_3^-}}{\gamma_{a,NaCO_3^-}(\mu)} + \frac{3a_{a,NaHCO_3}}{\gamma_{a,NaHCO_3}(\mu)} \end{array} \right) := \frac{a_{a,H_2O}}{\gamma_{a,H_2O}} + \delta C_{a,O(-2)}. \quad (8)$$

The total aqueous calcium concentration is

$$C_{a,Ca(2)} := \frac{a_{a,Ca^{2+}}}{\gamma_{a,Ca^{2+}}(\mu)} + \frac{a_{a,CaHCO_3^+}}{\gamma_{a,CaHCO_3^+}(\mu)} + \frac{a_{a,CaOH^+}}{\gamma_{a,CaOH^+}(\mu)} + \frac{a_{a,CaCO_3}}{\gamma_{a,CaCO_3}(\mu)} + \beta_{Ca}/2. \quad (9)$$

where β_{Ca} is the equivalent fraction of calcium (see Definition in [7]). The total aqueous sodium concentration is

$$C_{a,Na(1)} := \frac{a_{a,Na^+}}{\gamma_{a,Na^+}(\mu)} + \frac{a_{a,NaCO_3^-}}{\gamma_{a,NaCO_3^-}(\mu)} + \frac{a_{a,NaHCO_3}}{\gamma_{a,NaHCO_3}(\mu)} + \beta_{Na}. \quad (10)$$

where β_{Na} is the equivalent fraction of sodium.

The total aqueous chloride concentration is

$$C_{a,Cl(-1)} := \frac{a_{a,Cl^-}}{\gamma_{a,Cl^-}(\mu)}. \quad (11)$$

3.2 Multiphase mass-balance equations with surface complexes

Carbon balance We can write the mass balance equation for carbon as

$$\begin{aligned} &\partial_t \left(\varphi C_{a,C(4)} S_w + \varphi c_{o,CO_2} S_o + (1-\varphi) \left(c_{r,CaCO_3} + Cal_{s,CO_3^-} \right) \right) \\ &+ \partial_x u \left(C_{a,C(4)} f_w + c_{o,CO_2} f_o \right) \\ &= \partial_x \left(\varphi \left(D_w S_w \partial_x C_{a,C(4)} + D_o S_o \partial_x c_{o,CO_2} \right) \right) + \\ &\partial_x \left(\mathcal{D} C_{a,C(4)} \partial_x S_w \right) + \partial_x \left(\mathcal{D} c_{o,CO_2} \partial_x S_o \right), \end{aligned} \quad (12)$$

where c_{o,CO_2} is the concentration of CO_2 in the oil phase. The surface master species are arbitrarily chosen to be $oil_{s,N}$, $oil_{w,COO}$, $Cal_{s,O}$, Cal_{w,CO_3}. This choice uses that the sum of the species derived from the master species is equal to the number of active sites, which is considered to be constant for two sets of adsorbed sites on the oil surface and two sets adsorbed onto the calcite surface. Note that $S_o = 1 - S_w$. The equilibrium conditions of the sorbed species are taken from [12].

Hydrogen balance In the same way we find for the total hydrogen balance

$$\begin{aligned} &\partial_t \left(\varphi C_{a,H(1)} S_w \right) + \partial_t \varphi \left(oil_{s,N-H^+} + oil_{w,COO-H} \right) S_o \\ &+ \partial_t (1-\varphi) \left(2Cal_{s,O-2H^+} + Cal_{s,O-H} + Cal_{w,CO_3^- - H} \right) \\ &+ \partial_x \left(u C_{a,H(1)} f_w \right) + \partial_x u \left(oil_{s,N-H^+} + oil_{w,COO-H} \right) f_o = \\ &\partial_x \left(\mathcal{D} C_{a,H(1)} \partial_x S_w \right) + \partial_x \left(\mathcal{D} \left(oil_{s,N-H^+} + oil_{w,COO-H} \right) \partial_x S_o \right) \\ &+ \partial_x \left(\varphi D_w S_w \partial_x C_{a,H(1)} \right) + \partial_x \left(\varphi D_o S_o \partial_x \left(oil_{s,N-H^+} + oil_{w,COO-H} \right) \right), \end{aligned} \quad (13)$$

where the surface master species are chosen to be $oil_{s,N-}$, $oil_{w,COO-}$, $Cal_{s,O-}$, $Cal_{w,CO_3^- -}$.

Oxygen balance In the same way we find for the total oxygen balance

$$\begin{aligned}&\partial_t\Big(\varphi\Big(C_{a,O(-2)}S_w+2c_{o,CO_2}S_o\Big)+(1-\varphi)\Big(3c_{r,CaCO_3}\\&+2\Big(Cal_{s,CO_3^-}\Big)\Big)\Big)+\partial_x u\left(C_{a,O(-2)}f_w+2c_{o,CO_2}f_o\right)\\&=\partial_x\left(\mathcal{D}C_{a,O(-2)}\partial_x S_w\right)+2\partial_x\left(\mathcal{D}c_{o,CO_2}S_o\partial_x S_o\right)\\&+\partial_x\varphi\left(D_w S_w\partial_x C_{a,O(-2)}+2D_o S_o\partial_x c_{o,CO_2}\right).\end{aligned}\tag{14}$$

Calcium balance For the total calcium we find

$$\begin{aligned}&\partial_t\left(\varphi \mathtt{S}_\mathtt{w}\mathtt{C}_{\mathtt{a,Ca(2)}}+\varphi \mathtt{S}_\mathtt{o}\left(\mathtt{oil}_{\mathtt{w,COO-Ca^+}}\right)\right.\\&\left.+(1-\varphi)\left(\mathtt{c}_{\mathtt{r,CaCO_3}}+\mathtt{Cal}_{\mathtt{w,CO_3-Ca^+}}\right)\right)+\partial_t\beta_{Ca}\\&\times\partial_x u\left(C_{a,Ca(2)}f_w\right)+\partial_x u\left(oil_{w,COO-Ca^+}\right)\\&\times f_o=\partial_x\left(\mathcal{D}C_{a,Ca(2)}\partial_x S_w\right)+\partial_x\left(\mathcal{D}oil_{w,COO-Ca^+}\partial_x S_o\right)\\&+\partial_x\left(\varphi D_w S_w\partial_x C_{a,Ca(2)}\right)+\partial_x\left(\varphi D_o S_o\partial_x oil_{w,COO-Ca^+}\right).\end{aligned}\tag{15}$$

Sodium, Chlorine and total oil equation For the sodium equation we obtain

$$\begin{aligned}&\partial_t\left(\varphi S_w C_{a,Na(1)}\right)+\partial_t\beta_{Na}+\partial_x\left(uC_{a,Na(1)}f_w\right)\\&=\partial_x\left(\mathcal{D}C_{a,Na(1)}\partial_x S_w\right)+\partial_x\left(\varphi D_w S_w\partial_x C_{a,Na(1)}\right).\end{aligned}\tag{16}$$

In the same way we obtain for the first order terms of the chlorine equation

$$\begin{aligned}&\partial_t\left(\varphi S_w C_{a,Cl(-1)}\right)+\partial_x\left(uC_{a,Cl(-1)}f_w\right)\\&=\partial_x\left(\mathcal{D}C_{a,Cl(-1)}\partial_x S_w\right)+\partial_x\left(\varphi D_w S_w\partial_x C_{a,Cl(-1)}\right).\end{aligned}\tag{17}$$

For the total oil, e.g., heptane we retain the first order terms

$$\begin{aligned}\partial_t\left(\varphi S_o c_{o,C(-4)}\right)+\partial_x\left(uc_{o,C(-4)}f_o\right)&=\partial_x\left(\mathcal{D}c_{o,C(-4)}\partial_x S_o\right)\\&+\partial_x\left(\varphi D_o S_o\partial_x c_{o,C(-4)}\right).\end{aligned}\tag{18}$$

The oil concentration can be obtained from the dissolved carbon dioxide concentration c_{o,CO_2} (proportional to c_{a,CO_2}) with the EOS

$$\frac{c_{o,C(-4)}}{c_{O,C(-4)}}+\frac{c_{o,CO_2}}{c_{O,CO2}}=1.\tag{19}$$

3.3 System of conservation laws

Based on Gibbs rule and assuming that sodium and chloride concentration are similar we consider four conservation laws, namely for total carbon, hydrogen−oxygen, chloride and decane. Each one consists of four terms, i.e. accumulation, convection, molecular diffusion and capillary diffusion. We neglect diffusion and capillarity effects.

We can write the mass balance equation for carbon as

$$\begin{aligned}&\partial_t\left(\varphi C_{a,C(4)}S_w+\varphi c_{o,CO_2}S_o+(1-\varphi)\left(Cal_{s,CO_3^-}\right)\right)\\&+\partial_x\left(u\left(C_{a,C(4)}f_w+c_{o,CO_2}f_o\right)\right)=0.\end{aligned}\tag{20}$$

For the total oil, e.g., heptane we obtain

$$\partial_t\left(\varphi S_o c_{o,C(-4)}\right)+\partial_x\left(uc_{o,C(-4)}f_o\right)=0.\tag{21}$$

In the same way we obtain the chlorine equation

$$\partial_t\varphi S_w C_{a,Cl(-1)}+\partial_x\left(uC_{a,Cl(-1)}f_w\right)=0.\tag{22}$$

To remove one balance equation, we combine the hydrogen and oxygen balance equations to a single equation, in such a way that the water concentration is eliminated. We do so because the water concentration is much higher than the other concentrations.

We subtract twice the oxygen equation from the hydrogen equation and obtain after substitution of Eqs. (13) and (14)

$$\begin{aligned}&\partial_t\left(2\delta C_{a,O(-2)}-\delta C_{a,H(1)}\right)S_w-\partial_t\varphi\left(oil_{s,N-H^+}+oil_{w,COO-H}\right)S_o\\&-\partial_t(1-\varphi)\left(2Cal_{s,O-2H^+}+Cal_{s,O-H}+Cal_{w,CO_3^--H}\right)\\&2\partial_t\left(\varphi\left(2c_{o,CO_2}S_o\right)+(1-\varphi)\left(3c_{r,CaCO_3}+2\left(Cal_{s,CO_3^-}\right)\right)\right)\\&+\partial_x u\left(4c_{o,CO_2}-oil_{s,N-H^+}-oil_{w,COO-H}\right)f_o\\&+\partial_x u\left(\left(2\delta C_{a,O(-2)}-\delta C_{a,H(1)}\right)f_w\right)=0.\end{aligned}\tag{23}$$

In more compact way the system of conservation laws (20) and (23) can be written

$$\partial_t\left(\varphi\rho_{w1}S_w+\varphi\rho_{o1}S_o+\rho_{r1}\right)+\partial_x\left(u\left(\rho_{w1}f_w+\rho_{o1}f_o\right)\right)=0,\tag{24}$$

$$\partial_t\left(\varphi\rho_{o2}S_o\right)+\partial_x\left(u\left(\rho_{o2}f_o\right)\right)=0,\tag{25}$$

$$\partial_t\left(\varphi\rho_{w3}S_w\right)+\partial_x\left(u\left(\rho_{w3}f_w\right)\right)=0,\tag{26}$$

$$\partial_t\left(\varphi\rho_{w4}S_w+\varphi\rho_{o4}S_o+\rho_{r4}\right)+\partial_x\left(u\left(\rho_{w4}f_w+\rho_{o4}f_o\right)\right)=0,\tag{27}$$

where the coefficient functions are defined by

$$\rho_{w1}=C_{a,C(4)},\ \rho_{o1}=c_{o,CO_2},\ \rho_{r1}=(1-\varphi)\left(Cal_{s,CO_3^-}\right),\tag{28}$$

$$\rho_{o2}=C_{a,C(-4)},\quad \rho_{w3}=C_{a,Cl},\tag{29}$$

$$\rho_{w4}=\left(2\delta C_{a,O(-2)}-\delta C_{a,H(1)}\right),$$

$$\rho_{o4} = \left(4c_{o,CO_2} - \left(oil_{s,N-H^+} + oil_{w,COO-H}\right)\right), \tag{30}$$

$$\rho_{r4} = (1-\varphi)\Big(4Cal_{s,CO_3^-} - \Big(2Cal_{s,O-2H^+} + Cal_{s,O-H} + Cal_{w,CO_3^- -H}\Big)\Big). \tag{31}$$

where ρ_{wi}, ρ_{oi} and ρ_{ri} depend on pH and $[Cl]$. It is possible to verify that when the chemical surface complexes are not present then system (24)-(27) is reduced to the system studied in [6].

3.4 Fractional flow

The fractional flows for water and oil are saturation-dependent functions defined as follows. We denote $S_e(S_w) = (S_w - S_{wr})/(1 - S_{wr} - S_{or})$, for $S_w \geq S_{wr}$ and $S_e = 0$ for $S_w < S_{wr}$; $k_{rw}(S_w) = k_w(S_e(S_w))^{n_w}$ and $k_{ro}(S_w) = k_o(1 - S_e(S_w))^{n_o}$ ($S_o = 1 - S_w$) ([25]). Here n_w and n_o are the Corey exponents. The parameters k_w and k_o are end point relative permeabilities of water and oil phases, respectively.

The water viscosity is taken as $\mu_w = 0.001$ and the oil viscosity as $\mu_o = 0.002$ when they are constant; then we have the fractional flow functions for the aqueous and oleic phases

$$f_w(S_w) = \frac{k_{rw}(S_w)/\mu_w}{(k_{rw}(S_w)/\mu_w + k_{ro}(1-S_w)/\mu_o)}, \quad \text{and} \quad f_o(S_w) = 1 - f_w(S_w), \tag{32}$$

where the water and oil permeabilities $k_{rw}(S_w)$ and $k_{ro}(S_o)$ are expressed in terms of their saturations; μ_w and μ_o are the viscosities of the aqueous and oleic phases. We disregard capillarity and diffusive effects.

In this work we consider the relation between relative permeability and low salinity from the ideas described in [35]. Such a relation is based on the definition of the weight parameter θ to modify rock and fluid properties regarding salinity level. This model considers salt as an aqueous component that can be transported and traced. In this relation the relative permeability functions depend on water saturation S_w and salinity. This relationship is defined by the upper (HL) and lower (LS) limits for salinity called high and low salinity limits, respectively. To do that Corey's coefficients are adjusted for low and high salt concentration.

The weighting function θ is introduced by a linear relationship among two values for residual oil saturation corresponding to high and low salinity limits

$$\theta = \frac{S_{or} - S_{orw}^{LS}}{S_{orw}^{HL} - S_{orw}^{LS}}, \tag{33}$$

where the parameter θ is used for interpolating between preset high and low salinity curves for relative permeability and capillary pressure

$$K_{wi}(S_w) = \theta K_{ri}^{HL}(S_w) + (1-\theta)K_{ri}^{LS}(S_w), \tag{34}$$

where $i = w, o$ for water and oil permeability, respectively. For high salinity regime we take $k_w = 0.25$, $k_o = 0.5$, $n_w = 3$ and $n_o = 2$, while for low salinity the values $k_w = 0.41$, $k_o = 0.5$, $n_w = 3$ and $n_o = 2$ are used. Furthermore, in this study, the upper limit used for salinity corresponds to maximum residual oil saturation ($S_{or}^H = 0.35$). The lower limit corresponds to minimum residual oil saturation ($S_{or}^L = 0.15$).

4 Surface complexation modeling

This module is described in Sections

In this study, we use SCM to predict the wettability alteration of minerals through TBP. Details of the procedure employed here can be found in [28, 51]. The geochemistry solver PHREEQC was utilized to calculate the concentrations of the complexes. This program uses as input the properties of formation water and oil components of the crude oil. The properties of the minerals for several formation waters and for two polar oil components in the crude oil acid (e.g., COOH and NH^+) are used here. We take the input data described in [24]. Input properties of Oil are depicted in Tables 1 and 2.

The total acidic number (TAN) and the total base number (TBN) are used to calculate the oil site density using the formulas (see [10])

$$N_{S,COOH} = 0.602 \times 10^6 \frac{TAN}{1000\, a_{oil}\, MW_{KOH}}, \tag{35}$$

$$N_{S,NH^+} = 0.602 \times 10^6 \frac{TBN}{1000\, a_{oil}\, MW_{KOH}}, \tag{36}$$

where $MW_{KOH} = 56.1 g/mol$ molecular weight of potassium hydroxide. Here a_{oil} $[m^2/g]$ denotes the specific area of oil, which we assume to be the same as its respective carbonate minerals in aqueous solutions taken from [67].

Input data sets corresponding to salt are chosen for several formation waters where the ion concentrations of Na^{2+} and Cl^- varies. The data are taken to yield the coefficients of system (24)-(27), which depend on the ion concentration chosen in this work to represent the variability of state space, i.e.,

Table 1 Properties of the minerals and the polar oil components

Oil	Density (g/cm^3) at 20^{o}C	TAN (mg KOH/g oil)	TBN (mg KOH/g oil)
1	0.86	0.1	1.9
2	0.9	0.38	2.3

Table 2 Surface density and area of the two types of oil

Surface	Site Density (site/nm^2)	Surface Area (m^2/g)	Mass (g)
Calcite	4.9	2.0	0.2
Oil 1=COOH	0.54	2.0	2.59
Oil 1=NH+	10.2	2.0	2.59
Oil 2=COOH	2.04	2.0	2.71
Oil 2=NH+	12.34	2.0	2.71

pH and Cl^-. Since we assume that the ion concentrations of Na^{2+} and Cl^- are similar in the simulations, these ion concentrations vary from 30 to 1290 mmol/kgw. In turn, the ion concentrations of Ca^{2+}, Mg^{2+} and SO_4^{2-} are taken as constant. The pH is taken to vary from 2.7 to 8. Carbon is also taken as a constant in this study. The data are summarized in Table 3.

4.1 Regression formulas Matlab, Eureqa and PHREEQC program

The expressions for the coefficients ρ_{wi}, ρ_{oi} and ρ_{ri} $(i = 1, \ldots, 4)$ in system (24)-(27) are obtained using the ion concentrations of the complexes with formulas given in 28-31. These coefficients can also be determined by allowing the other minerals as Ca^{2+} and Mg^{2+} to vary as well. In such a case, and in accordance with the generalized Gibbs rule, it is necessary to add other equations to the model and to increase the number of degrees of freedom. This useful procedure can be used to study enhanced oil recovery by Smart Water injection, which we will study in future work with the methodology explained here.

Processing of the PHREEQC output data is done with MATLAB program, by using the curve fitting tool.

Denoting the ion concentration of hydrogen and chloride by $x = pH$ and $y = [Cl]$ the formula of the coefficients for the case of Oil 1 are

$$\rho_{w1} = -8.247 \cdot 10^{-7}\, x^5 + 8.841 \cdot 10^{-9}\, x^4\, y + 2.472 \cdot 10^{-5}\, x^4 + 9.621 \cdot 10^{-9}\, x^3\, y^2 + 3.387 \cdot 10^{-9}\, x^3\, y - 2.803 \cdot 10^{-4}\, x^3 + 9.781 \cdot 10^{-6}\, x^2\, y^3 - 2.523 \cdot 10^{-5}\, x^2\, y^2 - 2.843 \cdot 10^{-5}\, x^2\, y + 0.0015\, x^2 - 5.102 \cdot 10^{-5}\, x\, y^4 + 4.901 \cdot 10^{-5}\, x\, y^3 + 8.39 \cdot 10^{-5}\, x\, y^2 + 9.35 \cdot 10^{-5}\, x\, y - 0.0036\, x + 1.49 \cdot 10^{-4}\, y^5 - 2.383 \cdot 10^{-4}\, y^4 + 1.341 \cdot 10^{-4}\, y^3 - 1.758 \cdot 10^{-4}\, y^2 - 1.601 \cdot 10^{-4}\, y + 0.007, \quad (37)$$

Table 3 Formation waters where chloride and sodium ion concentrations vary. Other minerals are fixed

Ion	Synthetic injected water(mmol/kgw)
Na^+	30-1290
Mg^{2+}	40
Ca^{2+}	20
Cl^-	30-1290
SO_4^{2-}	20

$$\rho_{o1} = -1.575 \cdot 10^{-5} x^4 y + 1.01 \cdot 10^{-4} x^4 - 1.83 \cdot 10^{-5} x^3 * y^2 + 3.95 \cdot 10^{-4} x^3 y - 0.002 x^3 + 3.9010 \cdot 10^{-6} x^2 y^3 + 2.644 \cdot 10^{-4} x^2 y^2 - 0.0034 x^2 y + 0.0132 x^2, + 1.747 \cdot 10^{-5} x y^4 - 1.0440 \cdot 10^{-4} x y^3 - 0.0011 x y^2 + 0.0115 x y - 0.0369 x + 4.917 \cdot 10^{-4} y^5 - 0.0014 y^4 + 0.0015 y^3 + 7.16 \cdot 10^{-4} y^2 - 0.0134 y + 0.046, \quad (38)$$

$$\rho_{r1} = -1.056 \cdot 10^{-10} x^5 + 1.526 \cdot 10^{-10} x^4 y + 3.667 \cdot 10^{-9} x^4 + 3.284 \cdot 10^{-10} x^3 y^2, -3.606 \cdot 10^{-9} x^3 y - 4.844 \cdot 10^{-8} x^3 - 6.403 \cdot 10^{-10} x^2 y^3 - 3.359 \cdot 10^{-9} x^2 y^2, +2.797 \cdot 10^{-8} x^2 y + 2.980 \cdot 10^{-7} x^2 - 3.184 \cdot 10^{-9} x y^4 + 1.668 \cdot 10^{-8} x y^3, -6.75 \cdot 10^{-9} x y^2 - 7.32 \cdot 10^{-8} x y - 8.22 \cdot 10^{-7} x + 1.03 \cdot 10^{-8} y^4 - 4.66 \cdot 10^{-8} y^3 + 4.384 \cdot 10^{-8} y^2 + 5.35 \cdot 10^{-8} y + 8.19 \cdot 10^{-7}, \quad (39)$$

$$\rho_{o2} = 3.742 \cdot 10^{-6} x^5 + 4.911 \cdot 10^{-6} x^4 * y - 1.278 \cdot 10^{-4} x^4 - 4.653 \cdot 10^{-6} x^3 y^2, -1.09 \cdot 10^{-4} x^3 y + 0.0016 x^3 - 3.25 \cdot 10^{-5} x^2 y^3 + 1.2 \cdot 10^{-4} x^2 y^2 + 8.35 \cdot 10^{-4} x^2 y, -0.0087 * x^2 + 9.718 \cdot 10^{-5} x y^4 + 1.862 \cdot 10^{-4} x y^3 - 7.897 \cdot 10^{-4} x y^2, -0.0025 x y + 0.022 x - 6.073 \cdot 10^{-4} y^4 + 4.18 \cdot 10^{-4} y^3 + 9.108 \cdot 10^{-4} y^2 + 0.0027 * y + 1.812, \quad (40)$$

$$\rho_{w3} = 0.37 y, \quad (41)$$

$$\rho_{w4} = 2.61 \cdot 10^{-4} x^5 + 1.67 \cdot 10^{-4} x^4 y - 0.0079 x^4 + 2.78 \cdot 10^{-5} x^3 y^2, -0.003 x^3 y + 0.0914 x^3 + 8.04 \cdot 10^{-4} x^2 y^3 - 0.0025 x^2 y^2 + 0.025 x^2 y - 0.51 x^2, -0.0038 x y^3 + 0.0113 x y^2 - 0.0744 x y + 1.3520 x + 0.0021 y^3 - 0.0072 y^2 + 0.0616 y - 2.5890, \quad (42)$$

$$\rho_{o4} = -5.701 \cdot 10^{-5} x^5 - 6.681 \cdot 10^{-5} x^4 * y + 0.0019 * x^4 - 7.327 \cdot 10^{-5} x^3 y^2 + 0.0017 x^3 y - 0.0231 x^3 + 9.061 \cdot 10^{-6} x^2 y^3 + 0.0011 x^2 y^2 - 0.0142 x^2 y + 0.1273 x^2 + 2.365 \cdot 10^{-5} x y^4 - 1.965 \cdot 10^{-4} x y^3$$

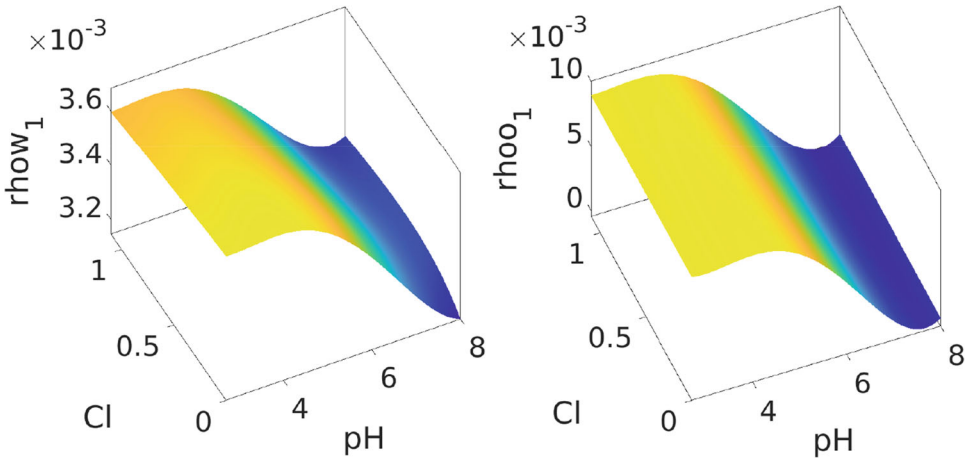

Fig. 1 Coefficients ρ_{w1}(left) and ρ_{o1}(right)

$$-0.0046xy^2 + 0.0483xy - 0.322x + 9.37 \cdot 10^{-4}y^5$$
$$-0.0023y^4 + 0.002y^3 + 0.006y^2 - 0.057y + 0.34, \quad (43)$$

$$\rho_{r4} = 5.86 \cdot 10^{-9}x^4 - 3.762 \cdot 10^{-10}x^3y - 1.33 \cdot 10^{-7}x^3$$
$$+1.228 \cdot 10^{-10}x^2y^2 + 3.162 \cdot 10^{-9}x^2y + 1.055 \cdot 10^{-6}x^2$$
$$+8.124 \cdot 10^{-9}xy^3 - 2.369 \cdot 10^{-8}xy^2 + 1.87 \cdot 10^{-8}xy$$
$$-3.282 \cdot 10^{-6}x - 4.032 \cdot 10^{-8}y^3 + 1.093 \cdot 10^{-7}y^2$$
$$-1.056 \cdot 10^{-7}y + 3.072 \cdot 10^{-6}. \quad (44)$$

The form of the function described for the above coefficients is the same for the two types of oil used in this study. These formulas show how much the pH affects the coefficients (see Figs. 1, 2, 3 and 4). In all coefficients the significant changes happen around $pH = 5$.

The coefficients in (37)-(44) are used as input to solve the system of conservation laws (24)-(27). First we use the numerical solution from the solver COMSOL, which is based on the finite element method. Second, we obtain the solution by the in house Riemann solver RPNfilho. To obtain a numerical solution we provide the coefficients and explore a set of parameters which permit to obtain stable solutions.

4.2 Wettability estimation

As suggested in [24], we assume that wettability is proportional to the Total Bound product (TBP). TBP estimation is based on the quantification with SCM of the attractive electrostatic forces existing between the rock-brine and the oil-brine interfaces. These forces are represented by Bound Product (BP), which is the product of the mole fractions of the oil (O_i) and mineral (m_i) sites with unlike charges [24] and it is given by the Equation:

$$BP = O_i * m_i \quad (45)$$

For a given mineral or rock, the sum of all the BP is the Total Bond Product (TBP) [24]. The SCM using PHREEQC solver predicts the oil adhesion onto a mineral or rock surface using the electrostatic pair linkages existing between the mineral-brine and oil-brine interfaces. It has been reported in the literature that the higher TBP corresponds to the

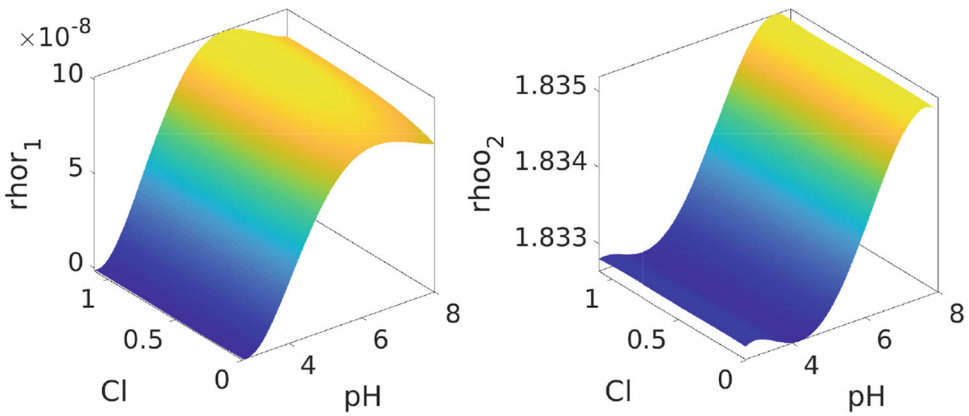

Fig. 2 Coefficients ρ_{r1}(left) and ρ_{o2}(right)

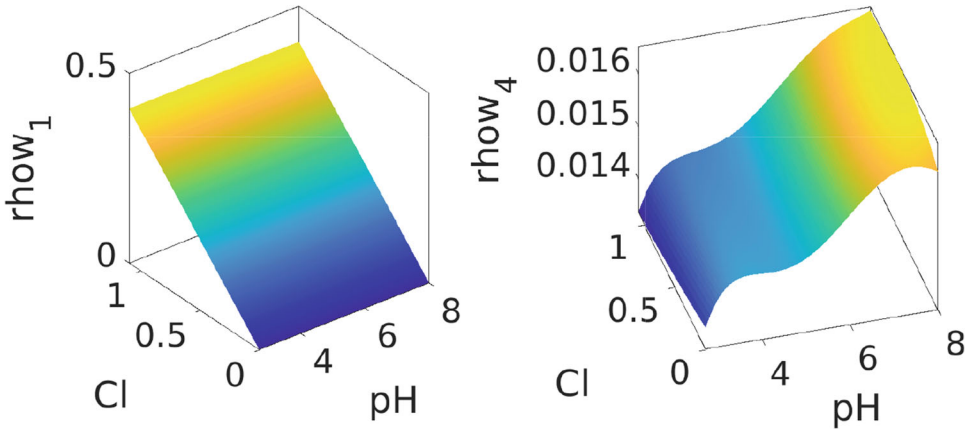

Fig. 3 Coefficients ρ_{w3}(left) and ρ_{w4}(right)

higher tendency for oil to be adsorbed onto the surface and vice-versa. The TBP can be written as:

$$
\begin{aligned}
TBP_1 &= (oil_{w,COO-}) * (Cal_{s,CaOH2+} + Cal_{w,CO3Ca+} \\
&\quad + Ca_{w,CO3Mg+}), \\
TBP_2 &= (oil_{s,NH+}) * (Cal_{w,CO3-} + Ca_{,s,CaO-} \\
&\quad + Cal_{s,CaCO3-} + Cal_{s,CaSO4-}), \\
TBP_3 &= oil_{w,COOCa+} * (Cal_{w,CO3-} + Cal_{s,CaO-} \\
&\quad + Cal_{s,CaCO3-} + Cal_{s,CaSO4-}), \\
TBP_4 &= oil_{w,COOMg+} * (Cal_{w,CO3-} + Cal_{s,CaO-} \\
&\quad + Cal_{s,CaCO3-} + Cal_{s,CaSO4-}), \\
TBP &= TBP_1 + TBP_2 + TBP_3 + TBP_4.
\end{aligned}
$$

The complexes of oil and rock are calculated with the PHREEQC solver with input values given in Tables 1-3.

Figures 5 and 6 shows TBP for oil type 1 and 2 respectively (see Table 1). In both cases, the TBP takes higher values for higher chloride concentration, which corresponds to what was reported in [62]. Their results indicate that a wettability shift from oil-wet to water-wet occurs when salinity is reduced.

The relation between TBP and pH is slightly different with respect to salinity ion concentration. Figure 6 shows that TBP has an oscillation with respect to pH, i.e., for $pH = 2.7$ a peak is observed in TBP, to later decrease and obtain a minimum at $pH = 3$. Subsequently, TBP increases until it reaches a peak above $pH = 5$, and then decreases for higher pH values. This behavior is maintained for temperatures of 95^oC but the peaks are more accentuated, see Fig. 7. These observed patterns of the TBP relationship with respect to pH are somewhat different from those reported by [62], where a wettability shift from water-wet to oil-wet can be achieved with increasing brine pH.

Our numerical experiment and the experimental result from [62] suggest that the relationship between TBP and wettability is not proportional to the quantity pH.

$$
\begin{aligned}
TBP(x, y) &= 0.0054x^4 + 0.0091x^3y - 0.1177x^3 \\
&\quad -0.0041x^2y^2 - 0.1433x^2y + 0.9304x^2 - 0.0469xy^3 \\
&\quad +0.1905xy^2 + 0.5342xy - 3.269x - 0.099y^4 \\
&\quad +0.615y^3 - 1.422y^2 + 0.2537y + 4.72. \qquad (46)
\end{aligned}
$$

Once wettability is estimated we use the procedure proposed in [13] to estimate the residual oil S_{or}. Given the

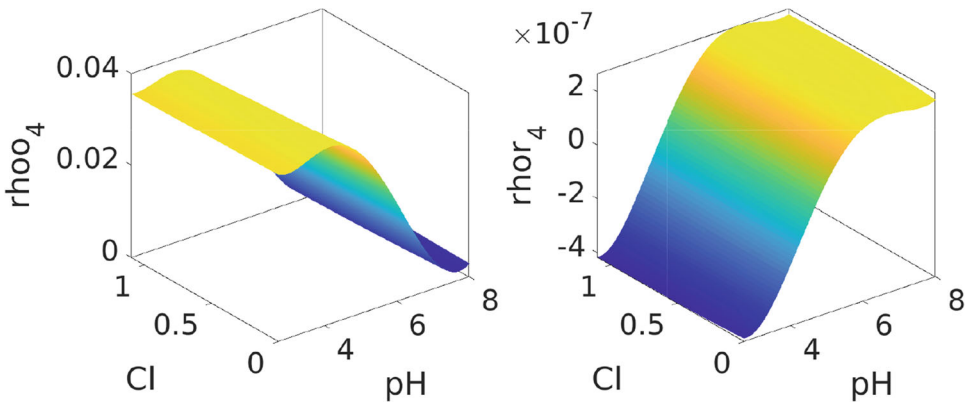

Fig. 4 Coefficients ρ_{o4}(left) and ρ_{r4}(right)

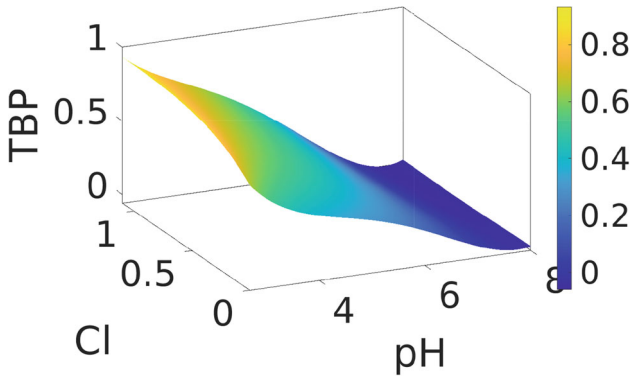

Fig. 5 Normalized TBP vs pH and Cl at temperature T=39^{o}C for the oil of type 1

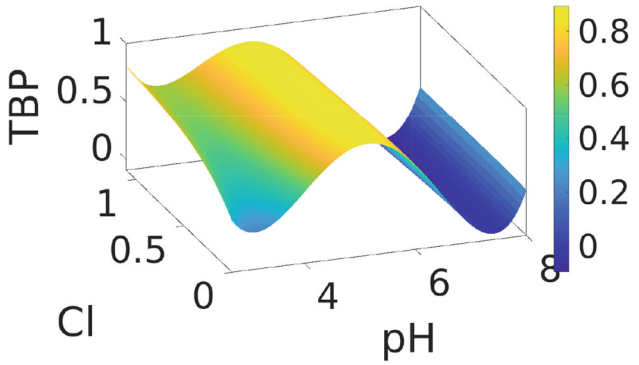

Fig. 7 Normalized TBP vs pH and Cl for temperature of T=95^{o}C

wettability index we obtain S_{or} from Fig. 8. Next, we obtain the initial water S_{wi} using the empirical relationship ([48])

$$S_{or} = 2.0698 S_{wi}^3 - 4.3857 S_{wi}^2 + 2.17419 S_{wi} + 0.148. \quad (47)$$

For estimating the residual oil S_{or}, we use the linear relationship with salt concentration given in [35].

Here, we propose a new formula for the parameter θ in Eq. (33) that takes into account the relationship between brine and pH as well as the wettability. The formula provides a direct method for calculating the parameter θ, allowing to consider the concentration of complexes in the fractional flow. The use of TBP in this context is a novel approach, as previous works have used total ionic strength instead (see e.g., [38]).

Formula for the parameter θ in (33) in term of TBP is given by

$$\theta = \frac{TBP(pH, Cl) - TBP_l}{TBP_h - TBP_l}, \quad (48)$$

where TBP is given in (46), TBP_l and TBP_h represent the TBP for the lower and higher brine concentration for a fixed pH. For example for Oil 1 in Table 1 and $pH = 4$ we have $TBP_l = 0.3841$ and $TBP_h = 0.534$. This formulation takes advantage of the established relationship between TBP and wettability. Therefore, once TBP is scaled, it serves to ensure the effect of salinity on the fractional flow function in an appropriate way.

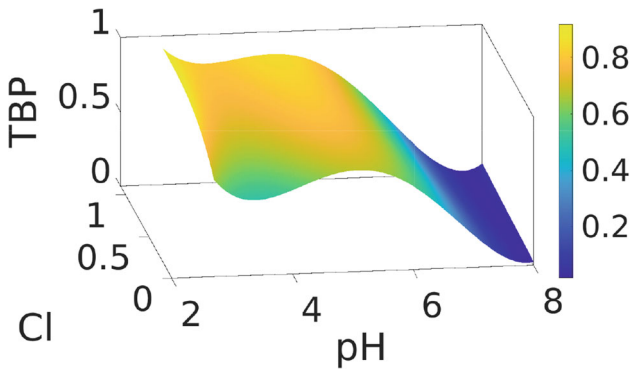

Fig. 6 Normalized TBP vs pH and Cl at temperature T=39^{o}C for the oil of type 2

5 Integration method of SCM with low salinity injection

This Section outlines the coupled modeling approach integrating carbonated water injection (CWI), low salinity injection and Surface Complexation Modeling (SCM). The interconnected elements forming this integration and their relationships are depicted in Fig. 9. This diagram represents the information flux relationships among the main components involved in this integration. We describe these components and their interactions below.

The Geochemical Modeling module is structured around a system of four conservation laws derived from a combination of primary Master species, equilibrium and balance equations

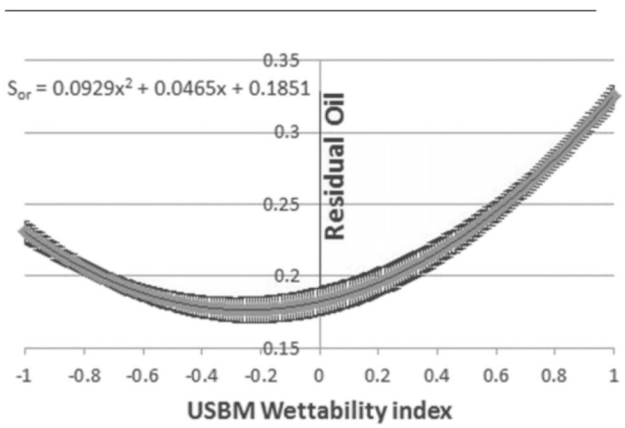

Fig. 8 Residual Oil Saturation as a function of the USBM (United States Bureau of Mines) wetting index [22]

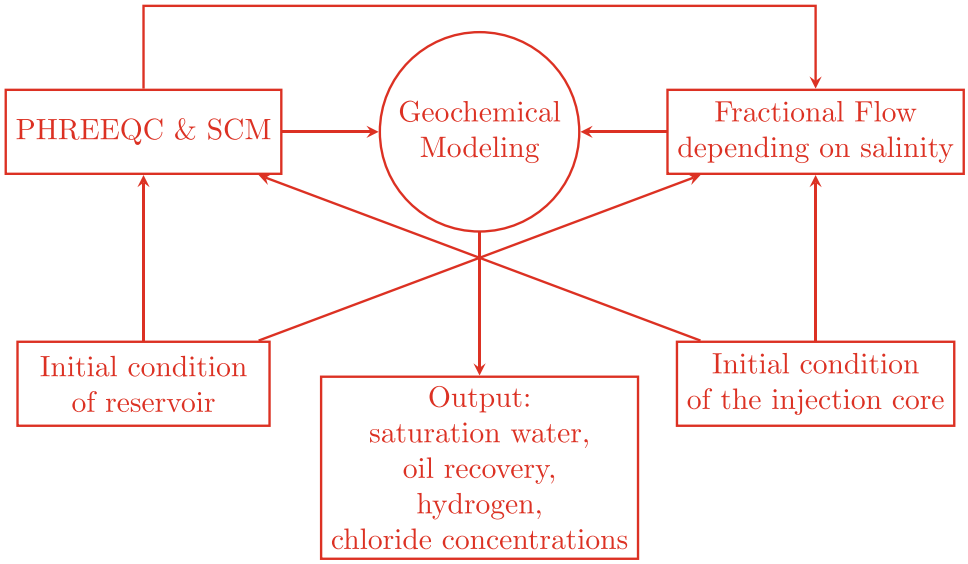

Fig. 9 Diagram of the main components of the integration of the Geochemical Model, Low Salinity Injection and SCM

of these species, surface complex sites, and adherence to the charge balance equation. A comprehensive analysis employing Gibbs' phase rule delineates the system's degrees of freedom. This module is described in Sections 2 and 3.1-3.3.

The PHREEQC & SCM module is a fundamental part of the geochemical modeling. This module thoroughly take into account water properties, initial mineral concentrations, temperature, pressure, and chemical equilibrium reactions. Furthermore, SCM incorporates initial conditions required to simulate the formation of complexes, such as surface area interactions, rock mineral composition, activities of mineral in water and petroleum composition.

Once the minerals and complexes concentrations are obtained, we proceed to the estimation of the conservation law coefficients depending on the chloride concentration (Cl) and pH. The calculation of the wettability is based on the Total Bound Product (TBP). Simultaneously, the wettability is used to determine the weight in the relative permeability for high and low salinity, which plays a crucial role in defining the fractional flow rate. This module is described in Section 4.

The Fractional Flow depending on salinity module takes into account the conditions for governing displacement processes. The fractional flow function derives information from the initial conditions of the reservoir, the activities of mineral in water, as well as the wettability parameter. This dependence is crucial in the Goechemical modeling integration. This module is described in Section 3.4.

The process described above is summarized in the following steps

1. **Step 1: Define initial reservoir conditions:** Connate water concentration, petroleum composition, surface area for oil components and porous rock, oil viscosity, absolute permeability, temperature, pressure, initial residual oil and porosity.
2. **Step 2: Determine water injection conditions:**
   - Initial concentrations of sulfates, magnesium, calcium, chlorine and sodium.
3. **Step 3:**
   (a) 3.1 Complete the geochemical solution using the PHREEQC program with all the input information determined in the initial steps,
   (b) 3.2 Determine coefficients for the Geochemical integration model depending on Cl and pH,
   (c) 3.3 Determine the wettability from the Total Bound Product (TBP), by using the concentrations of the surface complexes.
4. **Step 4:** Determine the fractional flow function using the initial salt concentration and the wettability.
5. **Step 5:** Solve the Geochemical model numerically and analytically.
6. **Step 6:** Process output information to determine oil recovery rate.

Several practical considerations to bear in mind in the process above are as follows: The integration of the low salinity, SCM, and the wettability occurs primarily in the fractional flow function, in Step 4. Besides, the presence of the surface complexes in the model also induces a change in the system of conservation laws, introducing a coefficient ρ_{ri} that represents the effect of considering complexes in Step 3.1.

Numerical experiments suggest that only slight variations in Darcy's velocity (u) occur. Therefore, in our simulations, this parameter is taken as a constant, facilitating the stabilization of the numerical scheme used.

The analytical solution is attained through the wave curve method. The essential elements for its use are described in the Section that follows, along with a summary of the technique. On the other hand, the numerical solution is obtained using the COMSOL version 6.1 program, which applies the refined Finite Element Method to the system of conservation laws of the Geochemical integration model.

6 Solving the Riemann-Goursat problem by MOC

Once we have determined the coefficients of the system of conservation laws (24)-(27) and fixed the fractional flow function f_w in (32) with θ given in (48), we can find the solution of such a system. Notice that the fractional flow has been determined taking into account the wettability values (through TBP), which in turn are estimated from the complexes. This solution of the system will allow us to determine the influence of the reduction of salt concentration at the point of injection.

The basis for MOC for the Riemann-Goursat problem is to assume that the independent variables (s_w, pH, Cl, u) are functions of the variable $\xi = x/t$, which is possible because the Riemann solution are scale invariant under the map $(t, x) \to (\alpha t, \alpha x)$; then we can take $U = (s_w, pH, Cl, u)(x, t) = (s_w, pH, Cl, u)(x(\xi), t(\xi)) = (s_w, y, u)(\xi)$ with characteristic lines $\xi = x/t$. If we assume that the functions $U(\xi) = (s_w(\xi), y(\xi), u(\xi))$ are differentiable along the characteristic lines, the following generalized eigenvalue equation for characteristics values holds

$$Ar = \lambda Br, \quad \text{where} \quad A = \partial F/\partial U, \quad B = \partial G/\partial U. \tag{49}$$

The eigenvector r is parallel to $dU/d\xi$, so the rarefaction curves are tangent to the characteristic field given by the normalized eigenvector r.

The physical model consists of four unknowns states variables $s_w, pH, [Cl], u$ satisfying system (24)-(27). The system has four equations with the unknown variables (s, y, u) with $y = (y_1, y_2) = (pH, [Cl])$ given by

$$\begin{aligned}&\frac{\partial}{\partial t}(\varphi\rho_{wj}(y)s_w + \varphi\rho_{oj}(y)s_o + (1-\varphi)\rho_{rj}(y))\\ &+\frac{\partial}{\partial x}((u)(\rho_{wj}(y)f_w + \rho_{oj}(y)f_o) = 0.\end{aligned} \tag{50}$$

We take $s = s_w$, $f = f_w$, $s_o = 1 - s$ and $f_o = 1 - f_w$. The accumulation G and flux functions $\hat{F} = (u/\phi)F$ are given by

$$G_j = \varphi\rho_{wj}(y)s_w + \varphi\rho_{oj}(y)s_o + (1-\varphi)\rho_{rj}(y) \tag{51}$$

$$F_j = \rho_{wj}(y)f_w + \rho_{oj}(y)f_o \tag{52}$$

The index w (water) is often replace by the index a (aqueous phase), and the index $j = 1, \cdots, 4$ is used to denote chemical species.

The main features in the 1-D Riemann solutions of hyperbolic systems are the rarefaction and shock curves. The rarefactions are obtained from integral curves of the line fields, given by the eigenvectors of system (49), where the matrices A, B represent the Jacobian matrices $A = D\hat{F}$ and $B = DG$ for the flux $\hat{F}$ and the accumulation G. For system (50), the matrices B, A are given by

$$B_{i,1} = [\rho_i], \quad B_{i,k+1} = \frac{\partial\rho_{wi}}{\partial y_k}s + \frac{\partial\rho_{oi}}{\partial y_k}s_o + \frac{\partial\rho_{ri}}{\partial y_k}, \text{ and } B_{i,n+1} = 0. \tag{53}$$

$$\begin{aligned}A_{i,1} &= (u/\phi)[\rho_i]\frac{\partial f}{\partial s}, \quad A_{i,k+1} = (u/\phi)\left(\frac{\partial\rho_{wi}}{\partial y_k}f + \frac{\partial\rho_{oi}}{\partial y_k}f_o\right)\\ &\text{and } A_{i,n+1} = F_i,\end{aligned} \tag{54}$$

in which $i = 1, \cdots, 4$, $k = 1, 2$ and

$$[\rho_i] = \rho_{wi} - \rho_{oi}. \tag{55}$$

From the Jacobian matrices, we obtain the eigenpairs which we have summarized in

Proposition 1 *The eigenpairs of the eigenvalue problem $A\vec{r} = \lambda B\vec{r}$, where the matrices B and A represent the Jacobian of the accumulation and flux terms of system (50) are the Buckley-Leverett eigenpairs $(\lambda_s, \vec{r}_s)$ given by*

$$\lambda_s = \frac{u}{\varphi}\frac{\partial f}{\partial s_w} \quad \textit{and} \quad \vec{r}_s = (1, 0, 0, 0)^T, \tag{56}$$

and two composition chemical with eigenpairs given by $(\lambda_\Lambda, \vec{r}_\Lambda)$:

$$\lambda_\Lambda = \frac{u}{\varphi}\frac{f - \Lambda}{s - \Lambda}. \tag{57}$$

We obtain Λ and $\vec{v} = (v_1, v_2)^T$ as the solutions of the compositional generalized eigenvalue problem

$$((\mathcal{A} + \mathcal{A}_1) - \Lambda(\mathcal{B} + \mathcal{B}_1))\vec{v} = 0, \tag{58}$$

where the matrices $\mathcal{A}, \mathcal{A}_1, \mathcal{B}$ and $\mathcal{B}_1$ are given in (88) and (90).

Moreover, we obtain $\vec{r}_\Lambda = (r_1, \cdots, r_4)$ as

$$r_4 = -\frac{\sum_2^3 \mathcal{G}^{(4)}_{4,j}v_{j-1}}{v_4}, \quad r_1 = \frac{\mathcal{G}_{1,4}r_4 - \sum_2^3 \mathcal{G}_{1,j}v_{j-1}}{\mathcal{G}_{1,1}}, \tag{59}$$

$$r_j = v_{j-1}, \quad \textit{for} \quad j = 2, 3. \tag{60}$$

where the matrices $\mathcal{G}$ and $\mathcal{G}^{(4)}_{4,j}$ evaluated at $\lambda = \lambda_\Lambda$ are given in (61) and (77)-(79).

Proof of Proposition

The idea of the proof consist of reducing the matrix $\mathcal{G}$ by continuous application of Gauss procedure leaving the matrix as a reduced matrix where the eigenvalues and eigenvectors are obtained easily.

To obtain the eigenvalues we solve $det(A-\lambda B)=0$, where $A-\lambda B=\mathcal{G}$, and $\mathcal{G}=(\mathcal{G}_{i,j})$ for $i,j=1,\cdots,4$. Here we use an auxiliary variable k that ranges from 1 to 2 and we write $\mathcal{G}_{i,j}$ as:

$$\mathcal{G}_{i,1}=[\rho_i]\xi_1,\quad \mathcal{G}_{i,k+1}=\frac{\partial\rho_{wi}}{\partial y_k}\xi_2+\frac{\partial\rho_{oi}}{\partial y_k}\xi_3-\lambda\frac{\partial\rho_{ri}}{\partial y_k}\quad\text{and}\quad \mathcal{G}_{i,4}=F_i, \tag{61}$$

where we define the auxiliary variables

$$\xi_1=\left(u\frac{\partial f}{\partial s}-\lambda\right),\quad \xi_2=(uf-\lambda s)\quad\text{and}\quad \xi_3=(uf_o-\lambda s_o). \tag{62}$$

For calculations purposes, that we do in the next proofs, it is useful to define the following functions γ_{ij}, ϱ_{ij}, ν_i, ϑ_{ij} and ς_{ij} for $i=1,\cdots,4$, $j=1,2$ as

$$\gamma_{ij}=\frac{\partial\rho_{wi}}{\partial y_j}[\rho_1]-\frac{\partial\rho_{w1}}{\partial y_j}[\rho_i],\ \varrho_{ij}=\frac{\partial\rho_{oi}}{\partial y_j}[\rho_1]-\frac{\partial\rho_{o1}}{\partial y_j}[\rho_i], \tag{63}$$

$$\pi_{ij}=\frac{\partial\rho_{ri}}{\partial y_j}[\rho_1]-\frac{\partial\rho_{r1}}{\partial y_j}[\rho_i],\quad \nu_i=[\rho_1]F_i-[\rho_i]F_1, \tag{64}$$

$$\vartheta_{ij}=\gamma_{ij}\nu_4-\gamma_{4,j}\nu_i,\quad \varsigma_{ij}=\varrho_{ij}\nu_4-\varrho_{4,j}\nu_i, \tag{65}$$

$$\tau_{ij}=\pi_{ij}\nu_4-\pi_{4,j}\nu_i. \tag{66}$$

All these coefficients ((63)- (66)) depend only of the variables y. Now, we are able to perform the proof os results in the text.

1) Substituting the i-th row of matrix (61), for $i=2,\cdots,4$, by the sum of the first row of $(A-\lambda B)$ (the elements of which are given by (61)) multiplied by $-[\rho_i]$ with its i-th row multiplied by $[\rho_1]$, we obtain, for $j=1,2$ and $i=2,3,4$

$$\mathcal{G}\sim\begin{pmatrix}\mathcal{G}_{1,1} & \mathcal{G}_{1,j+1} & \mathcal{G}_{1,4}\\ \mathbb{O} & \mathcal{G}^{(1)}_{i,j+1} & \mathcal{G}^{(1)}_{i,4}\end{pmatrix}. \tag{67}$$

Here $\mathbb{O}$ is the column vector of three zeros and block matrices $(\mathcal{G}^{(1)}_{i,j+1})$ and $(\mathcal{G}^{(1)}_{i,4})$ for $i=2,3,4$ and $j=1,2$ are the block matrices whose elements are given by

$$\mathcal{G}^{(1)}_{i,j+1}=\left(\gamma_{ij}\xi_2+\varrho_{ij}\xi_3-\pi_{ij}\lambda\right)_{1\le j\le 2}\quad\text{and}\quad \mathcal{G}^{(1)}_{i,4}=\nu_i, \tag{68}$$

where γ_{ij}, ϱ_{ij} π_{ij} and ν_i are given by Eq. (63) and (64). Notice here that if $[\rho_i]$, given y (55), is zero for some index i, the corresponding position in the first column is zero and we do not need to perform calculations to vanish this position. Moreover, if $[\rho_1]$ is zero, we exchange the position of row 1 with another row to obtain a non-zero pivot.

2) Now, we substitute i-th row of (67), for $i=2,3$, by the sum of the four row of (67) multiplied by $-\nu_i$ with the i-th row of (67) multiplied by ν_4, and we obtain for $j=1,2$ and $i=2,3$

$$\mathcal{G}\sim\begin{pmatrix}\mathcal{G}_{1,1} & \mathcal{G}_{1,j+1} & \mathcal{G}_{1,4}\\ \mathbb{O} & \mathcal{G}^{(2)}_{i,j+1} & \mathbb{O}\\ 0 & \mathcal{G}^{(2)}_{4,j+1} & \nu_4\end{pmatrix}. \tag{69}$$

Here $\mathbb{O}$ is the column vector of two zeros and $(\mathcal{G}^{(2)}_{i,j+1})$ and $(\mathcal{G}^{(1)}_{4,j+1})$ for $i=2,3$ and $j=1,2$ are the block matrices given by

$$\mathcal{G}^{(2)}_{i,j+1}=\vartheta_{ij}\xi_2+\varsigma_{ij}\xi_3-\tau_{ij}\lambda,\ \mathcal{G}^{(2)}_{4,j+1}=\left(\gamma_{4j}\xi_2+\varrho_{4j}\xi_3-\pi_{4j}\lambda\right), \tag{70}$$

where ϑ_{ij}, ς_{ij} and τ_{ij} are given by (65) and (66), for $i=1,\cdots,4$, $j=1,2$.

3) Now, we substitute the i-th row of (69), for $i=2,3$, by the sum of the four row of (69) multiplied by $-\tau_{i1}$ with the i-th row of (69) multiplied by π_{41}, and we obtain for $j=1,2$ and $i=2,3$

$$\mathcal{G}\sim\begin{pmatrix}\mathcal{G}_{1,1} & \mathcal{G}_{1,j+1} & \mathcal{G}_{1,4}\\ \mathbb{O} & \mathcal{G}^{(3)}_{i,j+1} & \mathbb{O}\\ 0 & \mathcal{G}^{(3)}_{4,j+1} & \nu_4\end{pmatrix}. \tag{71}$$

Here $\mathbb{O}$ is the column vector of two zeros and $(\mathcal{G}^{(3)}_{i,j+1})$ and $(\mathcal{G}^{(3)}_{4,j+1})$ for $i=2,3$ and $j=1,2$ are the block matrices given by

$$\mathcal{G}^{(3)}_{i,2}=m_{i1}\xi_2+n_{i1}\xi_3,\ \mathcal{G}^{(3)}_{i,3}=m_{i2}\xi_2+n_{i2}\xi_3-\alpha_{i2}\lambda \tag{72}$$

$$\mathcal{G}^{(3)}_{4,j+1}=\left(\gamma_{4j}\xi_2+\varrho_{4j}\xi_3-\pi_{4j}\lambda\right), \tag{73}$$

where

$$m_{ij}=\vartheta_{ij}\pi_{41}-\gamma_{4j}\tau_{i1},\ n_{ij}=\varsigma_{ij}\pi_{41}-\rho_{4j}\tau_{i1}, \tag{74}$$

$$\alpha_{i2}=\tau_{i2}\pi_{41}-\pi_{42}\tau_{i1},\ \alpha_{i1}=0. \tag{75}$$

and ϑ_{ij}, ς_{ij} and τ_{ij} are given by (64) and (66), for $i=1,\cdots,4$, $j=1,2$.

4) Now, we substitute third row of (71), by the sum of the second row of (71) multiplied by $-\alpha_{32}$ with the third row of (71) multiplied by α_{21}, and we obtain

$$\mathcal{G} \sim \begin{pmatrix} \mathcal{G}_{1,1} & \mathcal{G}_{1,j+1} & \mathcal{G}_{1,4} \\ \mathbb{O} & \mathcal{G}^{(4)}_{i,j+1} & \mathbb{O} \\ 0 & \mathcal{G}^{(4)}_{4,j+1} & \nu_4 \end{pmatrix}. \tag{76}$$

Here $\mathbb{O}$ is the column vector of two zeros and $(\mathcal{G}^{(4)}_{i,j+1})$ and $(\mathcal{G}^{(4)}_{4,j+1})$ for $i = 2, 3$ and $j = 1, 2$ are the block matrices given by:

$$\mathcal{G}^{(4)}_{2,2} = \bar{m}_{21}\xi_2 + \bar{n}_{21}\xi_3,\ \mathcal{G}^{(4)}_{2,3} = \bar{m}_{22}\xi_2 + \bar{n}_{22}\xi_3 + \alpha_{22}\lambda \tag{77}$$

$$\mathcal{G}^{(4)}_{3,2} = \bar{m}_{31}\xi_2 + \bar{n}_{31}\xi_3,\ \mathcal{G}^{(4)}_{3,3} = \bar{m}_{32}\xi_2 + \bar{n}_{32}\xi_3 \tag{78}$$

$$\mathcal{G}^{(4)}_{4,j+1} = \left(\gamma_{4j}\xi_2 + \varrho_{4j}\xi_3 + \pi_{4j}\lambda\right), \tag{79}$$

where

$$\bar{m}_{21} = m_{21}, \bar{n}_{21} = n_{21}, \bar{m}_{22} = m_{22}, \bar{n}_{22} = n_{22}, \tag{80}$$

and

$$\bar{m}_{31} = m_{31}\alpha_{21} - m_{21}\alpha_{32},\ \bar{n}_{31} = n_{31}\alpha_{21} - n_{21}\alpha_{32}. \tag{81}$$

$$\bar{m}_{32} = m_{32}\alpha_{21} - m_{22}\alpha_{32},\ \bar{n}_{32} = n_{32}\alpha_{21} - n_{22}\alpha_{32}. \tag{82}$$

5) Since $\mathcal{G}^{(4)}_{i,j+1}$ is block matrix, but this matrix appears in the rows 2 to 3 and columns 2 to 3 it is useful to define matrix $\left(G^{(4)}_{l,r}\right)$ for $l, r = 1, \cdots, 2$ from $\left(\mathcal{G}^{(4)}_{i,j+1}\right)$

$$G^{(4)}_{l,r} = \mathcal{G}^{(4)}_{l+1,r+1} \quad \text{for } l, r = 1, \cdots, 2. \tag{83}$$

From (76) and $\det(A - \lambda B) = 0$ a solution is $\xi_1 = 0$. Since ξ_1 is given by (62.a), thus we obtain the eigenpair $(\lambda_s, \vec{r}_s)$ given by (56). For this eigenpair, only saturation changes and we identify this family wave as *saturation wave*, or Buckley-Leverett type wave.
Using (76) and $det(A - \lambda B) = 0$, the other eigenvalues are obtained by solving

$$\det(G^{(4)}_{l,r}) = 0 \quad \text{for} \quad l, r = 1, 2, \tag{84}$$

with $G^{(4)}_{l,r}$ given by (77) and (78).

To obtain the corresponding eigenvalue, we substitute λ_Λ given by (57) into (84) and using that

$$\xi_2 = uf - \lambda_\Lambda s = u\frac{f(s-\Lambda) - (f-\Lambda)s}{s-\Lambda} = u\Lambda\frac{s-f}{s-\Lambda}. \tag{85}$$

$$\xi_3 = uf_o - \lambda_\Lambda s_o = u(1-f) - \lambda_\Lambda(1-s) = u(1-\Lambda)\frac{s-f}{s-\Lambda}. \tag{86}$$

Substituting ξ_2 and ξ_3 in (77) and (78) the matrix in (84) can be rewrite as

$$\begin{pmatrix} \bar{n}_{21} + \Lambda(m_{21} - \bar{n}_{21}) & \bar{n}_{22} + \Lambda(m_{22} - \bar{n}_{22}) \\ \bar{n}_{31} + \Lambda(m_{31} - \bar{n}_{31}) & \bar{n}_{32} + \Lambda(m_{32} - \bar{n}_{32}) \end{pmatrix} + \begin{pmatrix} 0 & \frac{\alpha_{22}(f-\Lambda)}{(s-f)} \\ 0 & 0 \end{pmatrix} \tag{87}$$

Denoting by

$$\mathcal{A} = \begin{pmatrix} \bar{n}_{21} & \bar{n}_{22} \\ \bar{n}_{31} & \bar{n}_{32} \end{pmatrix} \quad \text{and} \quad \mathcal{B} = -\begin{pmatrix} m_{21} - \bar{n}_{21} & m_{22} - \bar{n}_{22} \\ m_{31} - \bar{n}_{31} & m_{32} - \bar{n}_{32} \end{pmatrix}, \tag{88}$$

we obtain

$$\mathcal{A} - \Lambda\mathcal{B} + \begin{pmatrix} 0 & \frac{\alpha_{22}(f-\Lambda)}{(s-f)} \\ 0 & 0 \end{pmatrix}. \tag{89}$$

Also, denoting by

$$\mathcal{A}_1 = \begin{pmatrix} 0 & \frac{\alpha_{22} f}{(s-f)} \\ 0 & 0 \end{pmatrix} \quad \text{and} \quad \mathcal{B}_2 = \begin{pmatrix} 0 & \frac{\alpha_{22}}{(s-f)} \\ 0 & 0 \end{pmatrix}, \tag{90}$$

we have

$$G^{(4)}_{l,r} = (\mathcal{A} - \Lambda\mathcal{B}) + (\mathcal{A}_1 - \Lambda\mathcal{B}_2), \tag{91}$$

where the matrix $\mathcal{A}$ and $\mathcal{B}$ only depend the variables y, while the matrix $\mathcal{A}_1$ and $\mathcal{B}_1$ depend on y and s.
In this notation is easy to verify that equation (84) is a quadratic equation in the variable Λ. Thus equation (58) is a (2) × (2) algebraic system. If we have two different roots, we obtain two more eigenvalues of form (57). We call each eigenvalues as λ_{Λ_i} for $i = 1, 2$.
Also, notice that if $\rho_{rj} = 0$ ($j = 1, \cdots, 4$) then $\alpha_{22} = 0$ and the corresponding roots of equation (84) only depend on the chemical variable y. In this case solution can be found more easily (see [4]).

6) The eigenvectors related with λ_Λ are obtained solving

$$\begin{pmatrix} \mathcal{G}_{1,1} & \mathcal{G}_{1,j+1} & \mathcal{G}_{1,4} \\ \mathbb{O} & \mathcal{G}^{(4)}_{i,j+1} & \mathbb{O} \\ 0 & \mathcal{G}^{(4)}_{4,j+1} & \nu_4 \end{pmatrix} \vec{r} = 0. \tag{92}$$

We can split the calculation of $\vec{r}$. First we obtain the coordinates (r_2, r_3) of eigenvector $\vec{r}_\Lambda = (r_1, r_2, r_3, r_4)$. To do our calculations, we define the auxiliary vector $\vec{v}$ of two coordinates, which is the solution of

$$\left(G^{(4)}_{l,r}\right) \vec{v}^T = 0 \quad \text{for} \quad l, r = 1, 2. \tag{93}$$

Using (85)-(86), we can see that (93), after simplifications is written again as (58).
The coordinates r_{n+1} and r_1 are obtained by solving the first and the last equations of (92) and using (85)-(86), after some tedious calculations, we obtain Eqs. (59)-(60). □

The integral curves $\mathcal{W}^s$ and $\mathcal{W}^\Lambda$ associated to $\vec{r}_s$ and $\vec{r}_\Lambda$ are obtained by integrating the ODEs

$$d(s, y, u)/d\xi = \vec{r}_s \text{ and } \frac{d(s, y, u)}{d\xi} = \vec{r}_\Lambda. \tag{94}$$

From (94)a, we obtain the Buckley-Leverett(B-L) wave, where only the saturation changes, which is denotes by $\mathcal{R}_s$. Moreover, the solution of (94)b determines the waves associated to λ_Λ denotes by $\mathcal{R}_\Lambda$. Here, we do the technical proofs of results which appear in paper [4, 5]. These papers describe the numeric and theory of the main wave interactions of the system of conservation laws studied here.

6.1 Rankine-Hugoniot Locus

In this section we summarized how to calculated the discontinuous solution of the system of conservation laws studied here. Details of proof can be found in [5]. We denote $y = (pH, Cl)$ to gain in clearance.

The discontinuous solution of system of conservation laws (50) satisfy the Rankine-Hugoniot condition, i.e. for a given left and right state (s^-, y^-, u^-) and (s^+, y^+, u^+) respectively we have

$$u^+ F_i((s^+, y^+) - u^- F_i\left(s^-, y^-\right) = v^s \left(G_i\left(s^+, y^+\right) - G_i\left(s^-, y^-\right)\right), \tag{95}$$

with $i = 1, \ldots, n+1$ and v^s is the speed of discontinuity. Equation (95) can be rewritten as

$$\Phi_i.[v^s, u^+, u^-] = 0, \tag{96}$$

where $\Phi_i = (\Phi_{i1}, \Phi_{i2}, \Phi_{i2})$, with $\Phi_{i1} = s^+(\rho^+_{wi} - \rho^+_{oi}) + \rho^+_{oi} - (s^-(\rho^-_{wi} - \rho^-_{oi}) + \rho^-_{oi}) + (\rho^+_{ri} - \rho^+_{ri})$, $\Phi_{i2} = -(f^+(\rho^+_{wi} - \rho^+_{oi}) + \rho^+_{oi})$, $\Phi_{i3} = (f^+(\rho^-_{wi} - \rho^-_{oi}) + \rho^-_{oi})$ and $\rho^+ = \rho(y^+)$, $\rho^- = \rho(y^-)$, $f^+ = f\left(s^+, y^+\right)$, $f^- = f\left(s^-, y^-\right)$.

For each fixed state (s^-, y^-), the *Hugoniot-locus* $\mathcal{HL}(s^-, y^-)$ consist of all states (s^+, y^+) satisfying (96). In [43] is prove that

$$\mathcal{HL}\left(s^-, y^-\right) = \left\{\left(s^+, y^+\right) : det\left(\Phi^T_i, \Phi^T_k, \Phi^T_j\right) = 0\right\}, \tag{97}$$

for all the combination of distinct index $\{i, j, k\} \in \{1, 2, \cdots, n+1\}$. Also, we verify that instead to consider all the combination it is enough to reduce $n-1$ equations. This results can summarized as follows: let i_1 and $i_2 \in \{1, 2, \cdots, n+1\}$ two indices such that Φ_{i_1} and Φ_{i2} are independent linearly, then Eq. (97) reduces to

$$\mathcal{HL}\left(s^-, y^-\right) = \left\{\left(s^+, y^+\right) : det\left(\Phi^T_k, \Phi^T_{i_1}, \Phi^T_{i_2}\right) = 0\right\}, \tag{98}$$

for $k \in \{1, 2, \cdots, n+1\}$ distinct of i_1 and i_2. Equation (98) represents a curve in the three dimensional space (s, y) consisting in the intersection of two surfaces.

For fixed (s^-, y^-), there exists a branch of $\mathcal{HL}(s^-, y^-)$ consisting of the states of the form $(s, y) \in \Omega$, with s variable and $y = y^-$. This branch is called *Buckley-Leverett or saturation branch*, and it is denoted by $\mathcal{H}_s$. The other branches are denoted by $\mathcal{H}_\Lambda$.

6.2 Bifurcation surfaces

To determine the solution to the Riemann problem, we need rarefactions, the Hugoniot locus, and bifurcation surfaces. *Bifurcation loci* divide the phase space into subregions in which the sequences of waves for the Riemann solutions are the same. Seeking such surfaces, we take the flux functions $f = f_w$ given in (32). Here we will only put a summary, details about the formulas and deduction can be found in [4].

6.2.1 Coincidence locus

For each Λ_i there exist a *coincidence locus*, which is denoted by Γ_{Λ_i}; it occurs where the eigenvalues λ_s and λ_{Λ_i} coincide, i.e., at the zero of

$$\mathcal{G}_{\Lambda_i}(s, y) = \frac{\partial f(s, y)}{\partial s} - \left(\frac{f(s, y) - \Lambda_i(s, y)}{s - \Lambda_i(s, y)}\right). \tag{99}$$

The coincidence between two different λ_{Λ_i}, with $i = 1, 2$ occurs in some special cases. The states where $\lambda_{\Lambda_i} = \lambda_{\Lambda_j}$, we have $f = s$ or $\Lambda_i = \Lambda_j$.

6.2.2 Inflection loci

Other structures appearing in this model are the inflection loci. The inflections are, generically, co-dimension 1 structures, in which the monotone increase of characteristic speed fails, i.e., $\nabla\lambda \cdot \vec{r} = 0$.

In this model, we have three fields. For the field λ_s, it is easy to see that $\nabla\lambda_s \cdot \vec{r}_s = \frac{1}{\varphi}\frac{\partial^2 f}{\partial s^2}$, thus the inflection locus consists of the states $s^* = s^*(y)$, satisfying $\frac{\partial^2 f}{\partial s^2}(s^*, \cdot) = 0$. We denote the inflection for the field $(\lambda_s, \vec{r}_s)$ as $\mathcal{I}_s$:

$$\mathcal{I}_s = \left\{(s^*, y) : \frac{\partial^2 f}{\partial s^2}(s^*, y) = 0\right\}. \tag{100}$$

The inflection locus I_{Λ_i} of field $(\lambda_{\Lambda_i}, \vec{r}_{\Lambda_i})$ satisfies $\nabla\lambda_{\Lambda_i} \cdot \vec{r}_{\Lambda_i}$. Expression for this loci can be found describe in [4].

6.3 Analytical solution

We are interested in the Riemann-Goursat problem for the system (24)-(27) with piecewise constant initial data

$$\begin{cases} L = (Sw_L, pH_L, Cl_L, u_L) \textbf{ if } x < 0, \\ R = (Sw_R, pH_R, Cl_R, \cdot) \textbf{ if } x > 0. \end{cases} \tag{101}$$

The Riemann solution is obtained by the wave curve method. The solution is constructed by means of a sequence of elementary waves w_k (shocks and rarefactions) for $k = 1, 2, \cdots, m$ and constant states U_k for $k = 1, 2, \cdots, p$, in which p is not known a priori.

At any rate, this sequence of waves can be written as

$$\mathcal{U}_L \equiv \mathcal{U}_0 \xrightarrow{w_1} \mathcal{U}_1 \xrightarrow{w_2} \cdots \xrightarrow{w_m} \mathcal{U}_m \equiv \mathcal{U}_R, \tag{102}$$

where $\mathcal{U} = (s, pH, Cl, u)$. In the Riemann solution it is necessary that the waves have increasing speed, satisfying the so called *geometrical compatibility*. Sometimes, this geometrical compatibility is sufficient to furnish existence and uniqueness of the solution. Moreover, this condition is used to select the physical sequence of waves for the Riemann solution. We do not go into details about the wave curve method in this paper. Details can be found in [4, 5].

The waves consist of the B-L saturation wave curve $\mathcal{R}_s$ where only the saturation varies, the shock wave curve $\mathcal{H}_s$, the locus where only the saturation varies and the chemical saturation wave curves $\mathcal{R}_{\Lambda_i}$ $(i = 1, 2)$ associated to the couple $(\lambda_{\Lambda_i}, r_{\Lambda_i})$. Moreover other compatible wave curves include the composite wave curve $C_s = \mathcal{R}_s \cup \mathcal{H}_s$, formed by a characteristic B-L shock curve, and the composite wave curves $C_{\Lambda_i} = \mathcal{R}_{\Lambda_i} \cup \mathcal{H}_{\Lambda_i}$, where $\mathcal{H}_{\Lambda_i}$ is a characteristic shock curve associated to the branch of the family λ_{Λ_i} with $i = 1, 2$ and the constant state $\mathcal{C}$.

Taking into account bifurcation surfaces, we solve the Riemann solution for a particular problem, where we are able to obtain the sequence of the wave curves, when these wave curves cross the inflection or coincidence loci.

7 Numerical solution

In this section we present the numerical solution for the system (24)-(27) by using COMSOL and the Riemann solver RPNfilho.

For the simulations by using the COMSOL software, the hardware employed consists of a computer equipped with a latest-generation Intel Core i7 processor and 32 GB of RAM. Each simulation requires approximately 3 hours of processing time. The numerical solution is validated against the semi-analytical solution obtained by an in-house Riemann solver developed in MATLAB based on the wave curve method. Obtaining the wave sequences in the semi-analytical solution is relatively fast, once the bifurcation surfaces are determined.

We solve the Riemann-Goursat problem for some particular initial (right) and injection (left) conditions for such system of equations. We do not impose any condition on the variable u_R in (101) because its value is obtained from the other variables together with the solution of the system. Physically, the left state represents the value of the variables pH, $[Cl]$, S_w and u at the injection point. The right state presents the initial condition of such variables in the reservoir. The states studied here correspond to typical values of interest for petroleum engineering.

We assume that the fluid is incompressible, but there is mass transfer between phases of the carbon dioxide and the partial molar volume differs between phases, thus a variable total Darcy velocity ensues.

7.1 RPNfilho and COMSOL solutions

We are interested in evaluating the salt concentrations reduction at the injection point. To do so, first we cross-validated the method and second we identify the main waves present in the simulation of relevant examples. Besides calculating the speeds of the water saturation front and of the saline front, we estimate the behavior of the pH.

In this simulation we take a reduction of 5% in the initial chloride concentration in the reservoir, which we take as 0.3 mole per kilogram of water. To the chloride concentration of 0.015 mole per kilogram of water corresponds an oil saturation $S_{or} = 0.228$ and an initial water $S_{wi} = 0.0398$. The

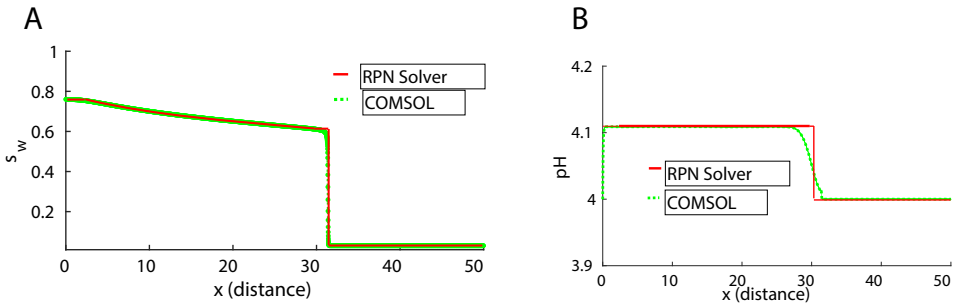

Fig. 10 a) Saturation profile from RPNfilho and COMSOL solvers, b) pH profile with RPNfilho and COMSOL solvers

initial condition for the Riemann problem consists of $L = (0.7604, 4.0, 0.015, 1.0\times10^{-5})$ and $R = (0.0398, 4.0, 0.3)$.

Figures 10-11 show the water saturation, the chloride and the pH profiles corresponding to the Riemann problem for a given L and R. We verify that in this example the solution of RPNfilho and COMSOL solvers match well. The saturation profile for both models coincide. The pH and chloride profiles match well except in the shock front solution.

The structure of the Riemann solution obtained by RPNfilho solver consists of a chemical 2-rarefaction wave, a constant state, a B-L rarefaction, a constant state, a 2-shock and a B-L shock. This sequence of waves can be represented schematically as $(L) \xrightarrow{\mathcal{R}_{\Lambda_2}} (A) \xrightarrow{\mathcal{R}_s} (B) \xrightarrow{\mathcal{H}_{\Lambda_2}} (C) \xrightarrow{\mathcal{H}_s} (R)$. This scheme means that from state L to the state $A = (0.7604, 4.12, 0.015)$ there exists a rarefaction $\mathcal{R}_{\Lambda_2}$ of the chemical family associated to eigenvalues λ_{Λ_2}. This wave is followed by a constant state from the state A to the state $B = (0.61, 4.12, 0.015)$, then we have a B-L rarefaction wave. Then we have another constant state followed by a type 2 shock to the point C. Immediately afterwards a constant state follows a B-L shock and reaches the right state R.

In the subsequent numerical examples the structure of the solution described above does not change. In these simulations only the relative position of the intermediate states vary when the initial conditions of the rock (right state) and the injection parameters (formation water, left state) change.

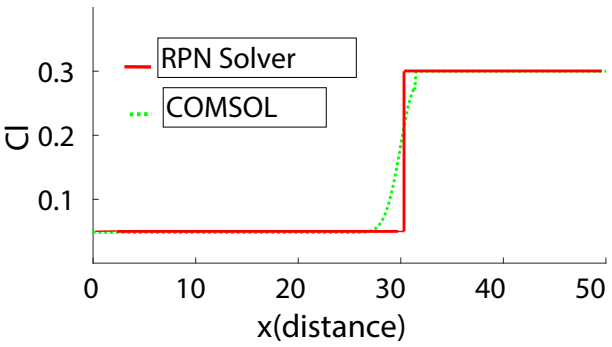

Fig. 11 Chloride profile from RPNfilho and COMSOL solver

7.2 Effect of brine reduction

In the following numerical experiments, we aim at investigating the effect of reducing the salinity on the oil recovery. In the first case, we assume a 5% reduction in the initial salt concentration, and the injection and initial states are defined by $L = (0.76, 4.0, 0.015, 1.0 \times 10^{-5})$ and $R = (0.0398, 4.0, 0.3)$, respectively. The corresponding residual oil saturation is $S_{or} = 0.228$ (as reported in [35]), and the initial water saturation is $S_{wi} = 0.0398$ (calculated using formula (47)).

In the second example, we assume a 20% reduction in the rock salt concentration, and the initial and injection states are defined by $R = (0.045, 4.0, 0.3)$ and $L = (0.76, 4.0, 0.06, 1.0 \times 10^{-5})$, respectively. The corresponding residual oil saturation is $S_{or} = 0.239$, and the initial water saturation is $S_{wi} = 0.045$ (calculated using formula (47)).

Figure 12 displays the profiles of water saturation S_w, pH, and chloride $[Cl]$ concentration for the two examples. Figure 13 shows the corresponding oil recovery for a 5% and 20% reduction in the rock salt concentration. We observed that a 5% reduction in salt concentration resulted in an increase in the oil recovery fraction of 0.066 with respect to the case of a 20% of salt concentration reduction. The oil recovery values obtained with our model are consistent with those reported in the experiments, as shown in studies such as [35, 39].

The Riemann solutions provide a numerical quantification and explanation of the influence of low salinity injection on the system state. In case (a) (as shown on the left side of Fig. 12), we present the solution for a 5% reduction in the salt concentration, while in case (b) (as shown on the right side of Fig. 12), we present the solution for a 20% reduction in the salt concentration. The Riemann solutions demonstrate the patterns of the system state, illustrating the effect of low salinity injection on the system.

In both cases (a) and (b) (as shown in Fig. 12), we observe the formation of three fronts, i.e., saturation S_w, pH and clhoride concentration $[Cl]$. The saline and pH fronts move at the same velocity, while the saturation front has a slightly higher velocity. The velocity of the saline and pH fronts is 4.05×10^{-5} for both cases, whereas the velocity of the

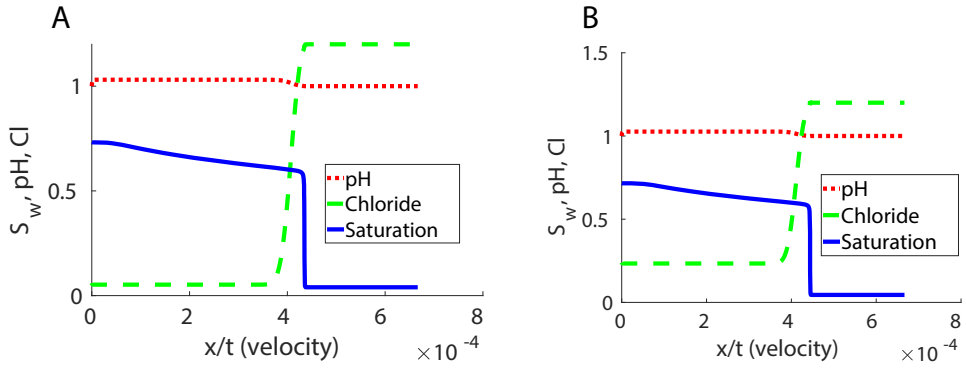

Fig. 12 The figures show profiles of the saturation S_w, scaled pH ($pH/4$), and scaled chloride concentration ($[Cl]*4$) at different velocities for a 5% and 20% reduction in salt concentration (left and right figures, respectively). The velocity of the saline and pH fronts are 4.05×10^{-5} and 4.08×10^{-5}, respectively, for the 5% reduction case, and the velocity of the saturation front is 4.34×10^{-5}. For the 20% reduction case, the velocity of the saline and pH fronts are 4.08×10^{-5}, while the velocity of the saturation front is 4.44×10^{-5}

saturation front is 4.34×10^{-5} for case (a) and 4.44×10^{-5} for case (b).

The increase in pH and the location of the front in pH close to the saturation front can be explained by the fact that pH controls the number of surface species at the interfaces of the oil/brine and the brine/carbonate (see e.g., [68]). This behavior of pH and of the saline front can also be explained by the fact that pH and salinity are among the most prominent factors affecting the wettability state of a crude oil/brine/rock system during waterflooding operations ([52]).

Another experiment was conducted to calculate the residual oil by changing the types of oil 1 and 2 presented in Table 1. However, no significant changes were observed for the type of oil studied in this experiment.

We confirmed that the coupling of SCM and compositional modeling accurately reproduces the main effects observed in the experiments, including wettability, residual oil, and connate water saturation as the main factors responsible for oil recovery. The processes controlling wettability and surface complexes are the change in pH and the formation of a pH front.

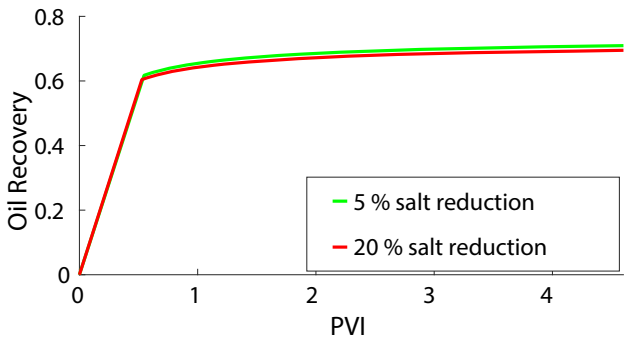

Fig. 13 Evaluating oil recovery with a decrease of 5% and 20% in salt concentration

8 Conclusion

This study quantifies the TBP of surface complexes and of wettability to estimate the effect of reducing rock salt concentration on permeability, and consequently, on oil recovery. We use a combination of SCM and compositional modeling to analyze the influence of wettability, residual oil, and connate water saturation on enhanced oil recovery. Our model reveals the presence of a shock in the saturation profile, with higher oil recovery being responsible for this phenomenon. We also observe a pH wave in a constant pH flood, salt formation at the front, and a jump in water saturation. The Riemann solution confirms the occurrence of pH variations numerically using COMSOL and RPNfilho solvers, which is expected when surface complexes are formed.

Acknowledgements We would like to express our sincere gratitude to the reviewers for their constructive feedback and insightful comments, which greatly enhanced the quality and depth of our manuscript. The authors are grateful to Ali A. Eftekhari for reviewing the calculations carried out using the PHREEQC program. Additionally, they would like to thank Sergio Pilotto for his support and acknowledge the funding received from CAPES under grant 88881.156518/2017-01 and CAPES/NUFFIC grant 88887.156517/2017-00, CNPq under grants 405366/2021-3 and 306566/2019-2, and FAPERJ under grants E-26/210.738/2014, E-26/202.764/2017, and E-26/201.159/2021.

Declarations

There are no conflicts of competing interests.

References

1. Alvarez, A.C., Bruining, J., Lambert, W.J., Marchesin, D.: Analytical and numerical solutions for carbonated waterflooding. Comput. Geosci. **22**(2), 505–526 (2018)
2. Al-Shalabi, E.W., Sepehrnoori, K., Delshad, M., Pope, G.: A novel method to model low-salinity-water injection in carbonate oil reservoirs. SPE J. **20**(05), 1154–1166 (2015)
3. Al-Shalabi, E.W., Sepehrnoori, K., Pope, G.: Geochemical interpretation of low-salinity-water injection in carbonate oil reservoirs. SPE J. **20**(06), 1212–1226 (2015)
4. Alvarez, A.C., Bruining, J., Marchesin, D.: Nonlinear wave interactions in geochemical modeling. J. Differ. Equ. **359**, 1–22 (2023)
5. Alvarez, A.C., Goedert, G.T., Marchesin, D.: Resonance in rarefaction and shock curves: local analysis and numerics of the continuation method. J. Hyperbolic Differ. Equ. **17**(04), 639–676 (2020)
6. Alvarez, A.C., Blom, T., Lambert, W.J., Bruining, J., Marchesin, D.: Analytical and numerical validation of a model for flooding by saline carbonated water. J. Pet. Sci. Eng. **167**, 900–917 (2018)
7. Appelo, C., Anthony, J., Postma, D.: Geochemistry, Groundwater and Pollution. Taylor & Francis (2005)
8. Appelo, C.A.J.: Cation and proton exchange, pH variations, and carbonate reactions in a freshening aquifer. Water Resour. Res. **30**(10), 2793–2805 (1994)
9. Ayirala, S.C., Yousef, A.A.: A state-of-the-art review to develop injection-water-chemistry requirement guidelines for ior/eor projects. SPE Prod. Oper. **30**(01), 26–42 (2015)
10. Bonto, M., Eftekhari, A.A., Nick, H.M.: An overview of the oil-brine interfacial behavior and a new surface complexation model. Sci. Rep. **9**(1), 1–16 (2019)
11. Bordeaux-Rego, F., Mehrabi, M., Sanaei, A., Sepehrnoori, K.: Improvements on modelling wettability alteration by engineered water injection: surface complexation at the oil/brine/rock contact. Fuel. **284**, 118991 (2021)
12. Brady, P.V., Krumhansl, J.L., Mariner, P.E.: Surface complexation modeling for improved oil recovery. In: SPE Improved Oil Recovery Symposium, pp. SPE 153744
13. Bruining, H.: Upscaling of Single-and Two-Phase Flow in Reservoir Engineering. CRC Press (2021)
14. Bryant, S.L., Schechter, R.S., Lake, L.W.: Interactions of precipitation/dissolution waves and ion exchange in flow through permeable media. AIChE J. **32**(5), 751–764 (1986)
15. Bryant, S.L., Schechter, R.S., Lake, L.W.: Mineral sequences in precipitation/dissolution waves. AIChE J. **33**(8), 1271–1287 (1987)
16. Buckley, S.E., Leverett, M.: Mechanism of fluid displacement in sands. Trans. AIME. **146**(01), 107–116 (1942)
17. Christensen, R.J.: Carbonated waterflood results–Texas and Oklahoma. In: Annual Meeting of Rocky Mountain Petroleum Engineers of AIME. OnePetro (1961)
18. De Nevers, N.: A calculation method for carbonated water flooding. Soc. Pet. Eng. J. **4**(01), 9–20 (1964)
19. Dong, Y., Dindoruk, B., Ishizawa, C., Lewis, E., Kubicek, T.: An experimental investigation of carbonated water flooding. In: SPE Annual Technical Conference and Exhibition. OnePetro
20. Dubey, S.T., Doe, P.H.: Base number and wetting properties of crude oils. SPE Reserv. Eng. **8**(3), 195–200 (1993)
21. Dumoré, J.M., Hagoort, J., Risseeuw, A.S.: An analytical model for one-dimensional, three-component condensing and vaporizing gas drives. Soc. Pet. Eng. J. **24**(02), 169–179 (1984)
22. Ebeltoft, E., Lomeland, F., Brautaset, A., Haugen, Å.: Parameter based scal-analysing relative permeability for full field application. In: International Symposium of the Society of Core Analysis, Avignon, France, pp. 8–11 (2014)
23. Elakneswaran, Y., Shimokawara, M., Nawa, T., Takahashi, S.: Surface complexation and equilibrium modelling for low salinity waterflooding in sandstone reservoirs. In: Abu Dhabi International Petroleum Exhibition & Conference. OnePetro (2017)
24. Erzuah, S., Fjelde, I., Omekeh, A.V.: Wettability estimation using surface-complexation simulations. SPE Reserv. Eval. Eng. **22**(02), 509–519 (2019)
25. Erzuah, S., Fjelde, I., Omekeh, A.V.: Modelling low-salinity waterflooding: effect of divalent cations and capillary pressure. J. Pet. Sci. Eng. **149**, 1–8 (2017)
26. Farajzadeh, R., Matsuura, T., van Batenburg, D., Dijk, H.: Detailed modeling of the alkali/surfactant/polymer (ASP) process by coupling a multipurpose reservoir simulator to the chemistry package PHREEQC. SPE Reserv. Eval. Eng. **15**(04), 423–435 (2012)
27. Foroozesh, J., Jamiolahmady, M., Sohrabi, M.: Mathematical modeling of carbonated water injection for EOR and CO2 storage with a focus on mass transfer kinetics. Fuel. **174**, 325–332 (2016)
28. Ginn, D.: Effects of potential determining ions and pH on the wettability of intermediate wet outcrop limestone. Master's thesis, University of Stavanger, Norway (2020)
29. Glimm, J.: Solutions in the large for nonlinear hyperbolic systems of equations. Commun. Pur. Appl. Math. **18**(4), 697–715 (1965)
30. Grogan, A.T., Pinczewski, W.V.: The role of molecular diffusion processes in tertiary CO_2 flooding. J. Pet. Technol. **39**(05), 591–602 (1987)
31. Hassan, A.M., Ayoub, M., Eissa, M., Bruining, H., Zitha, P.: Study of surface complexation modeling on a novel hybrid enhanced oil recovery (eor) method; smart-water assisted foam-flooding. J. Pet. Sci. Eng. **195**, 107563 (2020)
32. Helfferich, F.G.: The theory of precipitation/dissolution waves. AIChE J. **35**(1), 75–87 (1989)
33. Hirasaki, G., Zhang, D.L.: Surface chemistry of oil recovery from fractured, oil-wet, carbonate formation. In: International Symposium on Oilfield Chemistry. OnePetro (2003)
34. Honarpour, M.M.: Relative Permeability of Petroleum Reservoirs. CRC press (1986)
35. Jerauld, G.R., Webb, K.J., Lin, C.Y., Seccombe, J.C.: Modeling low-salinity waterflooding. SPE Reserv. Eval. Eng. **11**(06), 1000–1012 (2008)
36. Jerauld, G.R., Lin, C.Y., Webb, K.J., Seccombe, J.C.: Modeling low-salinity waterflooding. SPE Reserv. Eval. Eng. **11**(06), 1000–1012 (2008)
37. Johns, R.T., Dindoruk, B., Orr, F.M., Jr.: Analytical theory of combined condensing/vaporizing gas drives. SPE Adv. Technol. Ser. **1**(02), 7–16 (1993)
38. Korrani, A.K., Jerauld, G.R., Sepehrnoori, K.: Mechanistic modeling of low-salinity waterflooding through coupling a geochemical package with a compositional reservoir simulator. SPE Reserv. Eval. Eng. **19**(01), 142–162 (2016)
39. Korrani, A.K., Jerauld, G.R.: Modeling wettability change in sandstones and carbonates using a surface-complexation-based method. J. Pet. Sci. Eng. **174**, 1093–1112 (2019)
40. Kumar, S., Mandal, A.: A comprehensive review on chemically enhanced water alternating gas/CO_2 (CEWAG) injection for enhanced oil recovery. J. Pet. Sci. Eng. **157**, 696–715 (2017)
41. Lake, L.W.: Enhanced Oil Recovery. Prentice Hall Inc. (1989)
42. Lake, L.W., Johns, R.T., Rossen, W.R., Pope, G.A.: Fundamentals of Enhanced Oil Recovery. Society of Petroleum Engineers, Richardson (2014)
43. Lambert, W.J., Alvarez, A.C., Matos, V., Marchesin, D., Bruining, J.: Nonlinear wave analysis of geochemical injection for multicomponent two phase flow in porous media. J. Differ. Equ. **266**(1), 406–454 (2019)
44. Lax, P.D.: Hyperbolic systems of conservation laws II. Commun. Pur. Appl. Math. **10**(4), 537–566

45. Leverett, M.C.: Flow of oil-water mixtures through unconsolidated sands. Trans. AIME. **132**(01), 149–171 (1939)
46. Liu, T.P.: The Riemann problem for general 2×2 conservation laws. Trans. Am. Math. Soc. **199**, 89–112
47. Liu, T.P.: The Riemann problem for general systems of conservation laws. J. Differ. Equ. **18**(1), 218–234 (1975)
48. Lomeland, F., Ebeltoft, E., Hasanov, B.: A versatile representation of upscaled relative permeability for field applications (spe 154487). In: 74th EAGE Conference and Exhibition incorporating EUROPEC 2012, pp. cp–293. European Association of Geoscientists & Engineers (2012)
49. Lutzenkirchen, J.: Surface Complexation Modelling. Elsevier (2006)
50. Marmier, N., Dumonceau, J., Fromage, F.: Surface Complexation Modeling of yb (iii) sorption and desorption on hematite and alumina. J. Contam. Hydrol. **26**(1–4), 159–167 (1997)
51. Mehdiyev, F., Erzuah, S., Omekeh, A., Fjelde, I.: Surface Complexation Modelling of wettability alteration during carbonated water flooding. Energies. **15**(9), 3020 (2022)
52. Mehraban, M.F., Ayatollahi, S., Sharifi, M.: Experimental investigation on synergic effect of salinity and ph during low salinity water injection into carbonate oil reservoirs. J. Petrol. Sci. Eng. **202**, 108555 (2021)
53. Merkel, B.J.: Groundwater Geochemistry. Springer (2005)
54. Nowrouzi, I., Manshad, A.K., Mohammadi, A.H.: Effects of dissolved binary ionic compounds and different densities of brine on interfacial tension (ift), wettability alteration, and contact angle in smart water and carbonated smart water injection processes in carbonate oil reservoirs. J. Mol. Liq. **254**, 83–92 (2018)
55. Oleinik, O.A.: Discontinuous solutions of non-linear differential equations. Usp. Matematicheskikh Nauk. **12**(3), 3–73 (1957)
56. Omekeh, A., Friis, H.A., Fjelde, I., Evje, S.: Modeling of ion-exchange and solubility in low salinity water flooding. In: SPE Improved Oil Recovery Symposium. OnePetro (2012)
57. Parkhurst, D.L., Appelo, C.A.J.: User's guide to PHREEQC (version 2): A computer program for speciation, batch-reaction, one-dimensional transport, and inverse geochemical calculations (1999)
58. Parkhurst, D.L., Appelo, C.A.J.: Description of input and examples for PHREEQC version 3a computer program for speciation, batch-reaction, one-dimensional transport, and inverse geochemical calculations (2013)
59. Pope, G.A.: The application of fractional flow theory to enhanced oil recovery. Soc. Pet. Eng. J. **20**(03), 191–205 (1980)
60. Sanaei, A., Tavassoli, S., Sepehrnoori, K.: Investigation of modified water chemistry for improved oil recovery: application of DLVO theory and surface complexation model. Colloids Surf. A Physicochem. Eng. Asp. **574**, 131–145 (2019)
61. Sanaei, A., Varavei, A., Sepehrnoori, K.: Mechanistic modeling of carbonated waterflooding. J. Petrol. Sci. Eng. **178**, 863–877
62. Sari, A., Chen, Y., Xie, Q., Saeedi, A.: Low salinity water flooding in high acidic oil reservoirs: Impact of pH on wettability of carbonate reservoirs. J. Mol. Liq. **281**, 444–450 (2019)
63. Sheng, J.J.: Enhanced oil recovery field case studies. Gulf Professional Publishing (2013)
64. Sohrabi, M., Riazi, M., Jamiolahmady, M., Ireland, S., Brown, C.: Mechanisms of oil recovery by carbonated water injection. In: SCA annual meeting (2009)
65. Stumm, W., Morgan, J.J.: Aquatic Chemistry: Chemical Equilibria and Rates in Natural Waters, vol. 126. John Wiley & Sons (2012)
66. Welge, H.J., Johnson, E.F., Ewing, S.P., Jr., Brinkman, F.H.: The linear displacement of oil from porous media by enriched gas. J. Petrol. Technol. **13**(08), 787–796 (1961)
67. Wolthers, M., Charlet, L., Van Cappellen, P.: The surface chemistry of divalent metal carbonate minerals; a critical assessment of surface charge and potential data using the charge distribution multi-site ion complexation model. Am. J. Sci. **308**(8), 905–941 (2008)
68. Xie, Q., Sari, A., Pu, W., Chen, Y., Brady, P.V., Al Maskari, N., Saeedi, A.: pH effect on wettability of oil/brine/carbonate system: Implications for low salinity water flooding. J. Petrol. Sci. Eng. **168**, 419–425 (2018)
69. Yousef, A.A., Al-Saleh, S., Al-Jawfi, M.: Smart waterflooding for carbonate reservoirs: Salinity and role of ions. In: SPE Middle East Oil and Gas Show and Conference. OnePetro (2011)
70. Yousef, A.A., Al-Saleh, S., Al-Jawfi, M.: Improved/enhanced oil recovery from carbonate reservoirs by tuning injection water salinity and ionic content. In: SPE Improved Oil Recovery Symposium. OnePetro (2012)